

# A separation-of-variable dynamic stiffness matrix method for the free vibration of orthotropic rectangular thin plates

Shiyi Mei<sup>a</sup>, Colin Caprani<sup>a,\*</sup>, Daniel Cantero<sup>b</sup>

<sup>a</sup>*Department of Civil Engineering, Monash University, Melbourne, Victoria, Australia*

<sup>b</sup>*Department of Structural Engineering, Norwegian University of Science & Technology  
NTNU, Trondheim, Norway*

---

## Abstract

A separation-of-variable dynamic stiffness matrix method (SOV-DSM) is proposed for the free vibration analysis of an orthotropic rectangular thin plate with general homogeneous boundary conditions. Firstly, the exact SOV solution satisfying Rayleigh's principle is extended to handle arbitrary boundary conditions and then applied to develop closed-form dynamic stiffness formulations. Then, an enhanced Wittrick–Williams (W-W) algorithm is used to solve the eigenvalue problem rather than solving the highly nonlinear eigenvalue equations. The  $J_0$  count problem involved in applying the W-W algorithm is addressed by providing an explicit and closed-form expression for the  $J_0$  term based on the characteristics of the SOV solution. Furthermore, a numerical technique is provided to calculate the mode shape of the plate with any arbitrary boundary conditions. The accuracy of the proposed method is validated through numerical experiments by comparison with other analytical solutions.

---

\*Corresponding author

Email addresses: shiyi.mei1@monash.edu (Shiyi Mei), colin.caprani@monash.edu (Colin Caprani), daniel.cantero@ntnu.no (Daniel Cantero)

**1 1. Introduction**

2     Rectangular plates play an important role in many engineering fields, in-  
3     cluding civil, mechanical, and aerospace engineering [1]. The free vibration  
4     of plates has been a fundamental research problem for over two centuries.  
5     The earliest exact solutions for this problem are the Navier [2] and Levy  
6     [3] solutions, which require at least one pair of opposite edges to be simply  
7     supported or guided. To solve problems with other boundary conditions,  
8     approximate solutions such as the Rayleigh–Ritz method [4–8], the Galerkin  
9     method [9–13] and finite element method (FEM) [14–18] have been widely  
10    applied. For most approximation methods, beam functions [19–22], polyno-  
11    mials [23–27], trigonometric functions [28–32], and their combinations [33–  
12    37] are commonly used as the assumed approximate functions. The accuracy  
13    of these solutions depends on how well the assumed approximate functions  
14    represent the displacement of the plate.

15    Besides the approximation methods, several analytical methods have been  
16    developed over past decades, including the Kantorovich-Krylov method [38–  
17    44], the symplectic method [45–50], the separation-of-variable (SOV) method  
18    [46, 51–59], the dynamic stiffness matrix (DSM) method [60–71], and series  
19    expansion-based methods [72–90]. The series expansion-based methods in-  
20    clude the superposition method [72–77], Fourier series method [78–82], the  
21    finite integral transform method [83–87], and other series methods [88–90].  
22    These methods represent the plate displacement in terms of an infinite se-  
23    ries and mostly are capable of handling any general boundary conditions.  
24    However, sufficient truncation of the series is required to ensure the accuracy  
25    and convergence of the results, and the eigenvalue equation is generally dif-  
26    ficult to express explicitly. Therefore, solving the corresponding eigenvalue  
27    problem can be computationally expensive.

28    Despite being a powerful method for the dynamic analysis of plate as-  
29    semblies, the FEM requires a sufficient number of elements and is compu-  
30    tationally expensive to accurately capture higher-order modes. Thus, the

31 DSM method was developed as an accurate and efficient analytical approach  
32 to alternatively solve complex plate structures [63, 64]. The DSM can be  
33 considered as an analytical FEM since the mode functions of the plate are  
34 expressed by analytical solutions, where Levy-type solution [65] or compo-  
35 nents of Fourier series [66–70] are applied. To avoid solving the cumbersome  
36 transcendental frequency equation directly, the Wittrick-Williams (W-W) al-  
37 gorithm [91] can be applied to the eigenvalue problem. The W-W algorithm  
38 determines the lower and upper bounds of natural frequencies to arbitrary  
39 precision rather than solving the frequency equation directly. Thus, the DSM  
40 has the potential to be effectively and systematically solved using the W-W  
41 algorithm. However, a critical part in applying the W-W algorithm is to  
42 determine all natural frequencies of the fully clamped structure within the  
43 interested frequency range, *a priori*. Strategies such as using a sufficiently  
44 fine mesh or including a sufficient number of terms in series expansions [67]  
45 can ensure that all fully clamped frequencies are accounted for, thereby main-  
46 taining the accuracy of the algorithm. However, these approaches are compu-  
47 tionally expensive and complex, posing a significant obstacle to the wider  
48 adoption and application of the DSM method based on the W-W algorithm  
49 [92, 93]. To resolve the fully clamped plate problem, Liu and Banerjee [71]  
50 suggested that the frequencies can be indirectly obtained from the simply  
51 supported plate problem, where the Navier solution serves as the analytical  
52 solution. This idea provides a significant enhancement to the W-W algo-  
53 rithm, increasing the efficiency of applying DSM methods [69, 70]. However,  
54 most solutions applied in these DSM methods are not explicit and closed-  
55 form, but are expressed in an infinite series form, where a sufficient number  
56 of truncation terms might be required to ensure accuracy.

57 Inspired by the Navier and Levy solutions, Xing and Liu [51] proposed  
58 the SOV method, which provides concise and explicit eigensolutions. The  
59 mode shape function has a separable form,  $\phi(x)\psi(y)$ , requiring only one  $\phi(x)$   
60 and one  $\psi(y)$  for each mode order, allowing each eigenvalue equation to be

61 explicitly expressed. However, this SOV method is not suitable to deal with  
62 plates with free boundary conditions. Therefore, an extended SOV method  
63 [52, 53] based on the Rayleigh quotient was proposed to accommodate plates  
64 with all four classical boundary conditions, i.e., simply supported, clamped,  
65 guided, and free. Based on the Rayleigh quotient model, alternative iterative  
66 and improved SOV methods have been subsequently proposed [54]. Although  
67 SOV methods provide concise closed-form analytical solutions, they require  
68 solving a specific set of highly nonlinear eigenvalue equations for each type  
69 of boundary condition. However, even when considering only the four classic  
70 homogeneous cases, it becomes evident that 55 different boundary condition  
71 combinations exist for a rectangular plate, making the process tedious.

72 In this study, a separation-of-variable dynamic stiffness matrix (SOV-  
73 DSM) method is proposed to avoid solving transcendental eigenvalue equa-  
74 tions in SOV methods. It also fills the gap caused by the limitation of  
75 closed-form dynamic stiffness formulations available for existing plate struc-  
76 tures. Firstly, the SOV method is further extended to analyze the vibra-  
77 tions of plates with elastically restrained edges based on Rayleigh's principle.  
78 This extended SOV solution is then employed to construct dynamic stiffness  
79 matrices that accommodate general homogeneous boundary conditions. By  
80 taking advantage of both the SOV and DSM methods, an enhanced W-W  
81 algorithm is developed to solve the eigenvalue problem without directly solv-  
82 ing the eigenvalue equations. This enhanced approach resolves the challenge  
83 of determining fully clamped frequencies, also called the  $J_0$  count problem, a  
84 well-known limitation in the application of the W-W algorithm. Two types  
85 of explicit and closed-form expressions for the  $J_0$  term, based on specific  
86 support types such as simply supported, guided, or their combinations, are  
87 provided to improve the computational efficiency of the eigenvalue problem.  
88 In addition, a novel numerical technique is proposed to compute the mode  
89 shape coefficients.

90 The paper is structured as follows: Section 2 presents the SOV-DSM

91 formulations derived from the extended SOV method, which accommodates  
 92 elastically restrained boundary conditions. In Section 3, an enhanced W-  
 93 W algorithm that resolves the  $J_0$  count problem is provided to solve the  
 94 dynamic stiffness matrices. The explicit and closed-form expression for the  
 95  $J_0$  term is provided. In addition, a novel numerical technique is proposed to  
 96 compute the mode shape of the plate with arbitrary boundary conditions.  
 97 Section 4 validates the proposed method through numerical experiments by  
 98 comparison under several boundary conditions. Finally, the conclusions of  
 99 this paper are presented in Section 5.

100 **2. Separation-of-variable dynamic stiffness matrix formulation**

101 In this section, the SOV-DSM formulations for the free vibration analysis  
 102 of orthotropic rectangular thin plates are developed. Section 2.1 presents the  
 103 mathematical model of the extended separation-of-variable method. Then,  
 104 the SOV-DSM formulations in the  $x$ - and  $y$ -directions are developed sepa-  
 105 rately in Section 2.2 and Section 2.3, according to the boundary conditions  
 106 of the plate.

107 *2.1. Mathematical model for separation-of-variable method*

108 Consider a thin orthotropic rectangular plate of length  $2a$  and width  
 109  $2b$ , with all four edges restrained by vertical translational springs  $k^v$  and  
 110 rotational springs  $k^r$ , as shown in Figure 1. The coordinate origin is located  
 111 at the center of the plate.

112 The governing differential equation for the free vibration of a thin or-  
 113 thotropic plate is given by [54]:

$$D_{11} \frac{\partial^4 w}{\partial \xi^4} + 2D_3 \chi^2 \frac{\partial^4 w}{\partial \xi^2 \partial \eta^2} + D_{22} \chi^4 \frac{\partial^4 w}{\partial \eta^4} = \rho h a^4 \omega^2 w, \quad (1)$$

114 where  $\chi = a/b$  is the aspect ratio;  $\xi = x/a$  and  $\eta = y/b$  are the normalized

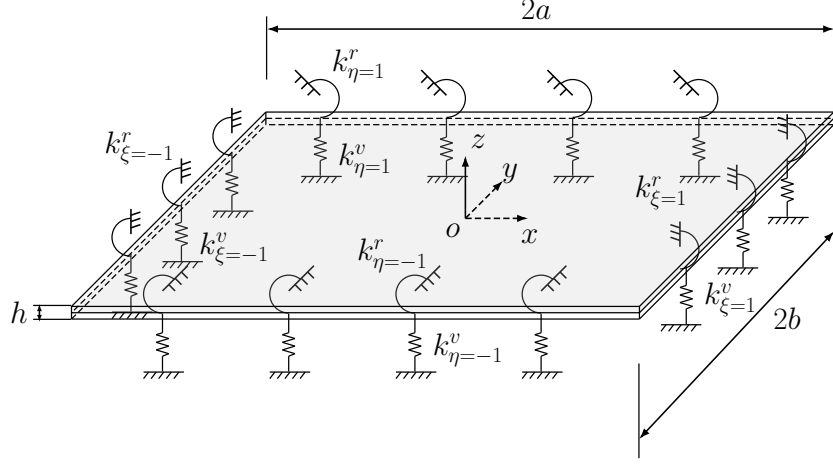


Figure 1: The orthotropic rectangular plate with all edges elastically restrained.

<sup>115</sup> coordinates, and the bending stiffness parameters are defined as:

$$\begin{aligned} D_{11} &= \frac{E_1 h^3}{12(1 - v_{12}v_{21})}, & D_{22} &= \frac{E_2 h^3}{12(1 - v_{12}v_{21})}, \\ D_{66} &= \frac{G_{12} h^3}{12}, & D_{12} &= v_{12} D_{22} = v_{21} D_{11}, & D_3 &= D_{12} + 2D_{66}, \end{aligned} \quad (2)$$

<sup>116</sup> where  $\rho$  and  $h$  denote the mass density and thickness of the plate, respectively;  
<sup>117</sup>  $E_1$  and  $E_2$  are the Young's moduli in the  $x$ - and  $y$ -directions, respectively;  
<sup>118</sup>  $G_{12}$  is the shear modulus, and  $v_{12}$  and  $v_{21}$  are the Poisson's ratios.

<sup>119</sup> Instead of solving the free vibration of the thin orthotropic plate using  
<sup>120</sup> Equation (1), it is suggested that the vibration of the thin plate can also be  
<sup>121</sup> solved using the Rayleigh quotient variational principle [52]:

$$\delta U = \delta T, \quad (3)$$

<sup>122</sup> where  $\delta$  denotes variation,  $U$  is the magnitude of the potential energy of the  
<sup>123</sup> plate, and  $T$  represents the magnitude of the kinetic energy of the plate. The

<sup>124</sup> potential energy of the plate can be expressed as [53]:

$$U^I = \frac{1}{2} \iint \left[ D_{11} \left( \frac{\partial^2 W}{\partial x^2} \right)^2 + 2D_{12} \frac{\partial^2 W}{\partial x^2} \frac{\partial^2 W}{\partial y^2} + D_{22} \left( \frac{\partial^2 W}{\partial y^2} \right)^2 + 4D_{66} \left( \frac{\partial^2 W}{\partial x \partial y} \right)^2 \right] dx dy. \quad (4)$$

<sup>125</sup> And the kinetic energy is:

$$T = \frac{1}{2} \iint \rho h \left( \frac{\partial W}{\partial t} \right)^2 dx dy. \quad (5)$$

<sup>126</sup> Assuming the solution of the deflection  $W(x, y; t) = w(x, y)e^{i\omega t}$  for har-  
<sup>127</sup> monic plate motion, where  $i = \sqrt{-1}$ ,  $w(x, y)$  is the mode shape, and  $\omega$  is the  
<sup>128</sup> radial frequency. By substituting  $W(x, y; t) = w(x, y)e^{i\omega t}$  into Equations (4)  
<sup>129</sup> and (5) and expressing the system in dimensionless coordinates, we have:

$$U^I = \frac{ab}{2} \iint \left[ \frac{D_{11}}{a^4} \left( \frac{\partial^2 w}{\partial \xi^2} \right)^2 + \frac{2D_{12}}{a^2 b^2} \frac{\partial^2 w}{\partial \xi^2} \frac{\partial^2 w}{\partial \eta^2} + \frac{D_{22}}{b^4} \left( \frac{\partial^2 w}{\partial \eta^2} \right)^2 + \frac{4D_{66}}{a^2 b^2} \left( \frac{\partial^2 w}{\partial \xi \partial \eta} \right)^2 \right] d\xi d\eta, \quad (6)$$

<sup>130</sup> and

$$T = \omega^2 \frac{ab}{2} \rho h \iint w^2 d\xi d\eta = \omega^2 T_0, \quad (7)$$

<sup>131</sup> where,  $T_0$  is defined as the coefficient of the kinetic energy.

<sup>132</sup> The separable form of the mode shape function  $w(\xi, \eta)$  is given by:

$$w(\xi, \eta) = \phi(\xi)\psi(\eta), \quad (8)$$

where  $\phi(\xi)$  and  $\psi(\eta)$  can be expressed as:

$$\phi(\xi) = A_1 \sin(\alpha_1 \xi) + A_2 \cos(\alpha_1 \xi) + A_3 \sinh(\beta_1 \xi) + A_4 \cosh(\beta_1 \xi), \quad (9a)$$

$$\psi(\eta) = B_1 \sin(\alpha_2 \eta) + B_2 \cos(\alpha_2 \eta) + B_3 \sinh(\beta_2 \eta) + B_4 \cosh(\beta_2 \eta). \quad (9b)$$

Based on Equation (3), the frequencies  $\omega_x$  and  $\omega_y$ , corresponding to the mode shapes  $\phi(\xi)$  and  $\psi(\eta)$ , respectively, are assumed to be independent of each other. This is a common and important assumption in SOV methods, and  $\omega_x$  and  $\omega_y$  can be different in a mathematical sense [53].

### 2.2. Dynamic stiffness matrix corresponding to $\omega_x$

For given general homogeneous boundary conditions, we can first assume that the mode shape  $\psi(\eta)$  corresponding to the  $y$ -direction is known. Supposing the edges of the plate in both the  $x$ - and  $y$ -directions are elastically restrained by homogeneous vertical translational and rotational springs. The vertical translational and rotational springs at the  $\xi = -1$  end are denoted as  $k_{\xi=-1}^v$  and  $k_{\xi=-1}^r$ , respectively, and at the  $\xi = 1$  end as  $k_{\xi=1}^v$  and  $k_{\xi=1}^r$ , respectively. Thus, the potential energy along the supported edge in the  $x$ -direction can be expressed by:

$$U^x = \int \left[ k_{\xi=-1}^r \left( \frac{\partial W}{\partial x} \right)^2 + k_{\xi=-1}^v (W)^2 \right]_{x=-a} dy + \int \left[ k_{\xi=1}^r \left( \frac{\partial W}{\partial x} \right)^2 + k_{\xi=1}^v (W)^2 \right]_{x=a} dy. \quad (10)$$

From Equation (10), the magnitude of potential energy along the plate edges in the  $x$ -direction, expressed in dimensionless coordinates, is obtained as:

$$U^x = ab \int \left[ \frac{k_{\xi=-1}^r}{a^3} \left( \frac{\partial w}{\partial \xi} \right)^2 + \frac{k_{\xi=-1}^v}{a} (w)^2 \right]_{\xi=-1} d\eta \\ + ab \int \left[ \frac{k_{\xi=1}^r}{a^3} \left( \frac{\partial w}{\partial \xi} \right)^2 + \frac{k_{\xi=1}^v}{a} (w)^2 \right]_{\xi=1} d\eta. \quad (11)$$

<sup>148</sup> The magnitude of total potential energy of the plate in the  $x$ -direction can  
<sup>149</sup> be obtained from Equations (6) and (11) as:

$$U = U^I + U^x \\ = \frac{ab}{2} \iint \left[ \frac{D_{11}}{a^4} \left( \frac{\partial^2 w}{\partial \xi^2} \right)^2 + \frac{2D_{12}}{a^2 b^2} \frac{\partial^2 w}{\partial \xi^2} \frac{\partial^2 w}{\partial \eta^2} + \frac{D_{22}}{b^4} \left( \frac{\partial^2 w}{\partial \eta^2} \right)^2 \right. \\ \left. + \frac{4D_{66}}{a^2 b^2} \left( \frac{\partial^2 w}{\partial \xi \partial \eta} \right)^2 \right] d\xi d\eta \\ + ab \int \left[ \frac{k_{\xi=1}^r}{a^3} \left( \frac{\partial w}{\partial \xi} \right)^2 + \frac{k_{\xi=1}^v}{a} (w)^2 \right]_{\xi=1} d\eta \\ + ab \int \left[ \frac{k_{\xi=-1}^r}{a^3} \left( \frac{\partial w}{\partial \xi} \right)^2 + \frac{k_{\xi=-1}^v}{a} (w)^2 \right]_{\xi=-1} d\eta \quad (12)$$

<sup>150</sup> By substituting Equation (8) into Equation (12), we have:

$$\begin{aligned}
U = & \frac{ab}{2} \int_{-1}^1 \left[ \frac{D_{11}}{a^4} I_1 \left( \frac{d^2 \phi}{d\xi^2} \right)^2 + \frac{2D_{12}}{a^2 b^2} I_2 \frac{d^2 \phi}{d\xi^2} \phi + \frac{D_{22}}{b^4} I_4 \phi^2 \right. \\
& \left. + \frac{4D_{66}}{a^2 b^2} I_3 \left( \frac{d\phi}{d\xi} \right)^2 \right] d\xi \\
& + ab I_1 \left[ \frac{k_{\xi=-1}^r}{a^3} \left( \frac{d\phi}{d\xi} \right)^2 + \frac{k_{\xi=-1}^v}{a} (\phi)^2 \right]_{\xi=-1} \\
& + ab I_1 \left[ \frac{k_{\xi=1}^r}{a^3} \left( \frac{d\phi}{d\xi} \right)^2 + \frac{k_{\xi=1}^v}{a} (\phi)^2 \right]_{\xi=1},
\end{aligned} \tag{13}$$

<sup>151</sup> where the integral parameters  $I_1$ ,  $I_2$ ,  $I_3$ , and  $I_4$  are defined and expressed in  
<sup>152</sup> Appendix A.

<sup>153</sup> By taking Equation (8) into account, the coefficient  $T_0$  of the kinetic  
<sup>154</sup> energy from Equation (7) for the plate in the  $x$ -direction can be expressed  
<sup>155</sup> as:

$$T_0 = \frac{ab}{2} \rho h \iint w^2 d\xi d\eta = \frac{ab}{2} \rho h I_1 \int_{-1}^1 \phi^2 d\xi. \tag{14}$$

<sup>156</sup> Taking the Rayleigh principle in the form:

$$\delta U = \omega_x^2 \delta T_0, \tag{15}$$

<sup>157</sup> and by substituting Equations (13) and (14) into Equation (15), and relieving

<sup>158</sup>  $\delta\phi$  and  $\delta\frac{d\phi}{d\xi}$  in Equation (15) by calculus of variations, yields:

$$\begin{aligned}
 0 = & \int_{-1}^1 \left[ \frac{D_{11}}{a^4} I_1 \frac{d^4\phi}{d\xi^4} + \left( \frac{2D_{12}}{a^2 b^2} I_2 - \frac{4D_{66}}{a^2 b^2} I_3 \right) \frac{d^2\phi}{d\xi^2} \right. \\
 & + \left. \left( \frac{D_{22}}{b^4} I_4 - \omega_x^2 \rho h I_1 \right) \phi \right] \delta\phi d\xi \\
 & + \frac{2k_{\xi=-1}^v}{a} I_1 (\phi \delta\phi)_{\xi=-1} + \frac{2k_{\xi=1}^v}{a} I_1 (\phi \delta\phi)_{\xi=1} \\
 & + \left[ \left( \frac{4D_{66}}{a^2 b^2} I_3 - \frac{D_{12}}{a^2 b^2} I_2 \right) \frac{d\phi}{d\xi} - \frac{D_{11}}{a^4} I_1 \frac{d^3\phi}{d\xi^3} \right] \delta\phi \Big|_{\xi=-1}^{\xi=1} \\
 & + \left( \frac{D_{12}}{a^2 b^2} I_2 \phi + \frac{D_{11}}{a^4} I_1 \frac{d^2\phi}{d\xi^2} \right) \delta \frac{d\phi}{d\xi} \Big|_{\xi=-1}^{\xi=1} \\
 & + \frac{2k_{\xi=-1}^r}{a^3} I_1 \left( \frac{d\phi}{d\xi} \delta \frac{d\phi}{d\xi} \right)_{\xi=-1} + \frac{2k_{\xi=1}^r}{a^3} I_1 \left( \frac{d\phi}{d\xi} \delta \frac{d\phi}{d\xi} \right)_{\xi=1}.
 \end{aligned} \tag{16}$$

<sup>159</sup> Thus, the governing differential equation in the  $x$ -direction can be obtained  
<sup>160</sup> from the integration part of Equation (16) as:

$$\frac{d^4\phi}{d\xi^4} + 2\chi^2 \left( \frac{D_{12}I_2}{D_{11}I_1} - 2\frac{D_{66}I_3}{D_{11}I_1} \right) \frac{d^2\phi}{d\xi^2} + \left( \chi^4 \frac{D_{22}I_4}{D_{11}I_1} - a^4 \Omega_x^4 \right) \phi = 0, \tag{17}$$

<sup>161</sup> where  $\Omega_x = \sqrt[4]{\omega_x^2 \rho h / D_{11}}$ . By substituting  $\phi(\xi) = A e^{\mu\xi}$  into Equation (17),  
<sup>162</sup> we obtain:

$$\mu^4 + 2\chi^2 \left( \frac{D_{12}I_2}{D_{11}I_1} - 2\frac{D_{66}I_3}{D_{11}I_1} \right) \mu^2 + \left( \chi^4 \frac{D_{22}I_4}{D_{11}I_1} - a^4 \Omega_x^4 \right) = 0. \tag{18}$$

<sup>163</sup> And so the solution for  $\mu$  can be expressed as:

$$\mu_{1,2} = \pm i\alpha_1, \quad \mu_{3,4} = \pm \beta_1, \tag{19}$$

where,

$$\alpha_1 = \chi \sqrt{\left( \frac{D_{12}I_2}{D_{11}I_1} - 2\frac{D_{66}I_3}{D_{11}I_1} \right)^2 - \frac{D_{22}I_4}{D_{11}I_1} + b^4\Omega_x^4 + \frac{D_{12}I_2}{D_{11}I_1} - 2\frac{D_{66}I_3}{D_{11}I_1}}, \quad (20a)$$

$$\beta_1 = \chi \sqrt{\left( \frac{D_{12}I_2}{D_{11}I_1} - 2\frac{D_{66}I_3}{D_{11}I_1} \right)^2 - \frac{D_{22}I_4}{D_{11}I_1} + b^4\Omega_x^4 - \frac{D_{12}I_2}{D_{11}I_1} + 2\frac{D_{66}I_3}{D_{11}I_1}}. \quad (20b)$$

- <sub>164</sub> The boundary conditions along the edges in the  $x$ -direction can be obtained  
<sub>165</sub> from the remaining  $\delta\phi$  and  $\delta\frac{d\phi}{d\xi}$  parts in Equation (16). The shear force  
<sub>166</sub> equilibrium can be obtained from the  $\delta\phi$  part:

$$\begin{aligned} & \left[ \left( \frac{4D_{66}}{a^2b^2}I_3 - \frac{D_{12}}{a^2b^2}I_2 \right) \frac{d\phi}{d\xi} - \frac{D_{11}}{a^4}I_1 \frac{d^3\phi}{d\xi^3} \right] \Big|_{\xi=-1}^{\xi=1} \\ & + \frac{2k_{\xi=-1}^v}{a} I_1(\phi)_{\xi=-1} + \frac{2k_{\xi=1}^v}{a} I_1(\phi)_{\xi=1} = 0, \end{aligned} \quad (21)$$

- <sub>167</sub> and from the  $\delta\frac{d\phi}{d\xi}$  part, the bending moment equilibrium is:

$$\begin{aligned} & \left( \frac{D_{12}}{a^2b^2}I_2\phi + \frac{D_{11}}{a^4}I_1 \frac{\partial^2\phi}{\partial\xi^2} \right) \Big|_{\xi=-1}^{\xi=1} \\ & + \frac{2k_{\xi=-1}^r}{a^3} I_1 \left( \frac{\partial\phi}{\partial\xi} \right)_{\xi=-1} + \frac{2k_{\xi=1}^r}{a^3} I_1 \left( \frac{\partial\phi}{\partial\xi} \right)_{\xi=1} = 0. \end{aligned} \quad (22)$$

Thus, we can obtain the shear force and bending moment equilibrium along

the edges  $\xi = -1$  and  $\xi = 1$  from Equations (21) and (22), respectively, as:

$$\frac{d^3\phi}{d\xi^3} - \chi^2 \left( \frac{4D_{66}I_3}{D_{11}I_1} - \frac{D_{12}I_2}{D_{11}I_1} \right) \frac{d\phi}{d\xi} + \frac{2a^3k_{\xi=-1}^v}{D_{11}}\phi = 0, \quad \xi = -1, \quad (23a)$$

$$\frac{d^2\phi}{d\xi^2} + \frac{\chi^2 D_{12}I_2}{D_{11}I_1}\phi - \frac{2ak_{\xi=-1}^r}{D_{11}}\frac{d\phi}{d\xi} = 0, \quad \xi = -1, \quad (23b)$$

$$\frac{d^3\phi}{d\xi^3} - \chi^2 \left( \frac{4D_{66}I_3}{D_{11}I_1} - \frac{D_{12}I_2}{D_{11}I_1} \right) \frac{d\phi}{d\xi} - \frac{2a^3k_{\xi=1}^v}{D_{11}}\phi = 0, \quad \xi = 1, \quad (23c)$$

$$\frac{d^2\phi}{d\xi^2} + \frac{\chi^2 D_{12}I_2}{D_{11}I_1}\phi + \frac{2ak_{\xi=1}^r}{D_{11}}\frac{d\phi}{d\xi} = 0, \quad \xi = 1. \quad (23d)$$

<sub>168</sub> Substituting Equation (9a) into Equation (23), and denoting  $k_{\xi}^{v*} \equiv \frac{2a^3k_{\xi}^v}{D_{11}}$ ,  
<sub>169</sub>  $k_{\eta}^{r*} \equiv \frac{2ak_{\xi}^r}{D_{11}}$ ,  $S_{\alpha_1} \equiv \sin \alpha_1$ ,  $C_{\alpha_1} \equiv \cos \alpha_1$ ,  $Sh_{\beta_1} \equiv \sinh \beta_1$ , and  $Ch_{\beta_1} \equiv \cosh \beta_1$ ,  
<sub>170</sub> we have:

$$\begin{bmatrix} \gamma_1 C_{\alpha_1} - k_{\xi=-1}^{v*} S_{\alpha_1} & \gamma_1 S_{\alpha_1} + k_{\xi=-1}^{v*} C_{\alpha_1} & \gamma_2 Ch_{\beta_1} - k_{\xi=-1}^{v*} Sh_{\beta_1} \\ \gamma_3 S_{\alpha_1} + k_{\xi=-1}^{r*} \alpha_1 C_{\alpha_1} & -\gamma_3 C_{\alpha_1} + k_{\xi=-1}^{r*} \alpha_1 S_{\alpha_1} & \gamma_4 Sh_{\beta_1} + k_{\xi=-1}^{r*} \beta_1 Ch_{\beta_1} \\ -\gamma_1 C_{\alpha_1} + k_{\xi=1}^{v*} S_{\alpha_1} & \gamma_1 S_{\alpha_1} + k_{\xi=1}^{v*} C_{\alpha_1} & -\gamma_2 Ch_{\beta_1} + k_{\xi=1}^{v*} Sh_{\beta_1} \\ \gamma_3 S_{\alpha_1} + k_{\xi=1}^{r*} \alpha_1 C_{\alpha_1} & \gamma_3 C_{\alpha_1} - k_{\xi=1}^{r*} \alpha_1 S_{\alpha_1} & \gamma_4 Sh_{\beta_1} + k_{\xi=1}^{r*} \beta_1 Ch_{\beta_1} \\ -\gamma_2 Sh_{\beta_1} + k_{\xi=-1}^{v*} Ch_{\beta_1} & -\gamma_4 Ch_{\beta_1} - k_{\xi=-1}^{r*} \beta_1 Sh_{\beta_1} & \\ -\gamma_2 Sh_{\beta_1} + k_{\xi=1}^{v*} Ch_{\beta_1} & \gamma_4 Ch_{\beta_1} + k_{\xi=1}^{r*} \beta_1 Sh_{\beta_1} & \end{bmatrix} \begin{Bmatrix} A_1 \\ A_2 \\ A_3 \\ A_4 \end{Bmatrix} = \begin{Bmatrix} 0 \\ 0 \\ 0 \\ 0 \end{Bmatrix}, \quad (24)$$

<sub>171</sub> or,

$$\mathbf{R}_x \mathbf{A} = \mathbf{0}, \quad (25)$$

<sup>172</sup> where,

$$\begin{aligned}\gamma_1 &= -\alpha_1^3 - \chi^2 \left( \frac{4D_{66}S_3}{D_{11}I_1} - \frac{D_{12}I_2}{D_{11}I_1} \right) \alpha_1, \\ \gamma_2 &= \beta_1^3 - \chi^2 \left( \frac{4D_{66}S_3}{D_{11}I_1} - \frac{D_{12}I_2}{D_{11}I_1} \right) \beta_1, \\ \gamma_3 &= -\alpha_1^2 + \frac{\chi^2 D_{12}I_2}{D_{11}I_1}, \\ \gamma_4 &= \beta_1^2 + \frac{\chi^2 D_{12}I_2}{D_{11}I_1}.\end{aligned}\tag{26}$$

<sup>173</sup> Note that the classic boundary conditions can be obtained by selecting  
<sup>174</sup> extremely large or small spring stiffness constants. For non-trivial solutions,  
<sup>175</sup> the characteristic equation or eigenvalue equation is obtained from the de-  
<sup>176</sup> terminant of the matrix  $\mathbf{R}_x$  in Equation (25), which must be zero. However,  
<sup>177</sup> solving these transcendental equations is cumbersome and so the DSM is  
<sup>178</sup> introduced to avoid such a computation.

<sup>179</sup> To develop the plate's dynamic stiffness matrix, with the help of Equa-  
<sup>180</sup> tion (9a), the vertical displacement and rotation corresponding to the mode  
<sup>181</sup> shape  $\phi(\xi)$  along the  $x$ -direction at edges  $\xi = -1$  and  $\xi = 1$  can be expressed  
<sup>182</sup> as:

$$\begin{Bmatrix} \phi_{\xi=-1} \\ \frac{d\phi}{d\xi}_{\xi=-1} \\ \phi_{\xi=1} \\ \frac{d\phi}{d\xi}_{\xi=1} \end{Bmatrix} = \begin{bmatrix} -S_{\alpha_1} & C_{\alpha_1} & -Sh_{\beta_1} & Ch_{\beta_1} \\ \alpha_1 C_{\alpha_1}/a & \alpha_1 S_{\alpha_1}/a & \beta_1 Ch_{\beta_1}/a & -\beta_1 Sh_{\beta_1}/a \\ S_{\alpha_1} & C_{\alpha_1} & Sh_{\beta_1} & Ch_{\beta_1} \\ \alpha_1 C_{\alpha_1}/a & -\alpha_1 S_{\alpha_1}/a & \beta_1 Ch_{\beta_1}/a & \beta_1 Sh_{\beta_1}/a \end{bmatrix} \begin{Bmatrix} A_1 \\ A_2 \\ A_3 \\ A_4 \end{Bmatrix}, \tag{27}$$

<sup>183</sup> or,

$$\delta_x = \mathbf{Q}_x \mathbf{A}. \tag{28}$$

<sup>184</sup> Solving for the eigenvector  $\mathbf{A}$ , and then substituting into Equation (25), we  
<sup>185</sup> obtain:

$$\mathbf{R}_x \mathbf{A} = \mathbf{R}_x \mathbf{Q}_x^{-1} \delta_x = \mathbf{0}. \tag{29}$$

186 where the dynamic stiffness matrix, denoted as  $\mathbf{K}_x = \mathbf{R}_x \mathbf{Q}_x^{-1}$ , can be ob-  
 187 tained from Equation (29). This matrix can be used to compute the natural  
 188 frequencies of the system instead of solving the eigenvalue equation, and the  
 189 method for the computation will be given in Section 3.

190 *2.3. Dynamic stiffness matrix corresponding to  $\omega_y$*

191 In this section, the mode shape  $\phi(\xi)$  derived in *Section 2.2* is utilized to  
 192 obtain the dynamic stiffness matrix in the  $y$ -direction. The vertical trans-  
 193 lational and rotational springs at  $\eta = -1$  are denoted as  $k_{\eta=-1}^v$  and  $k_{\eta=-1}^r$ ,  
 194 respectively, while those at  $\eta = 1$  are represented by  $k_{\eta=1}^v$  and  $k_{\eta=1}^r$ .

195 Following the same steps as for the  $x$ -direction, the Rayleigh principle is  
 196 expressed in the form:

$$\delta U = \omega_y^2 \delta T_0, \quad (30)$$

197 from which the governing differential equation in the  $y$ -direction for  $\psi$  is  
 198 obtained as:

$$\frac{d^4\psi}{d\eta^4} + \frac{2}{\chi^2} \left( \frac{D_{12}J_2}{D_{22}J_1} - 2 \frac{D_{66}J_3}{D_{22}J_1} \right) \frac{d^2\psi}{d\eta^2} + \left( \frac{D_{11}J_4}{\chi^4 D_{22}J_1} - \frac{b^4 D_{11}}{D_{22}} \Omega_y^4 \right) \psi = 0, \quad (31)$$

199 where  $\Omega_y = \sqrt[4]{\omega_y^2 \rho h / D_{11}}$ . By substituting  $\psi(\eta) = Be^{\lambda\eta}$  into Equation (31),  
 200 we get:

$$\lambda^4 + \frac{2}{\chi^2} \left( \frac{D_{12}J_2}{D_{22}J_1} - 2 \frac{D_{66}J_3}{D_{22}J_1} \right) \lambda^2 + \left( \frac{D_{11}J_4}{\chi^4 D_{22}J_1} - \frac{b^4 D_{11}}{D_{22}} \Omega_y^4 \right) = 0. \quad (32)$$

201 The solution for  $\lambda$  can be expressed as:

$$\lambda_{1,2} = \pm i\alpha_2, \quad \lambda_{3,4} = \pm \beta_2, \quad (33)$$

where,

$$\alpha_2 = \frac{1}{\chi} \sqrt{\sqrt{\left(\frac{D_{12}J_2}{D_{22}J_1} - 2\frac{D_{66}J_3}{D_{22}J_1}\right)^2 - \frac{D_{11}J_4}{D_{22}J_1} + \frac{a^4 D_{11}}{D_{22}} \Omega_y^4} + \frac{D_{12}J_2}{D_{22}J_1} - 2\frac{D_{66}J_3}{D_{22}J_1}}, \quad (34a)$$

$$\beta_2 = \frac{1}{\chi} \sqrt{\sqrt{\left(\frac{D_{12}J_2}{D_{22}J_1} - 2\frac{D_{66}J_3}{D_{22}J_1}\right)^2 - \frac{D_{11}J_4}{D_{22}J_1} + \frac{a^4 D_{11}}{D_{22}} \Omega_y^4} - \frac{D_{12}J_2}{D_{22}J_1} + 2\frac{D_{66}J_3}{D_{22}J_1}}. \quad (34b)$$

202 Similarly to the  $x$ -direction, from the shear force and bending moment  
203 equilibrium, and by denoting  $k_\eta^{v*} \equiv \frac{2b^3 k_\eta^v}{D_{22}}$ ,  $k_\eta^{r*} \equiv \frac{2bk_\eta^r}{D_{22}}$ ,  $S_{\alpha_2} \equiv \sin \alpha_2$ ,  $C_{\alpha_2} \equiv$   
204  $\cos \alpha_2$ ,  $Sh_{\beta_2} \equiv \sinh \beta_2$ , and  $Ch_{\beta_2} \equiv \cosh \beta_2$ , we obtain:

$$\begin{bmatrix} \zeta_1 C_{\alpha_2} - k_{\eta=-1}^{v*} S_{\alpha_2} & \zeta_1 S_{\alpha_2} + k_{\eta=-1}^{v*} C_{\alpha_2} & \zeta_2 Ch_{\beta_2} - k_{\eta=-1}^{v*} Sh_{\beta_2} \\ \zeta_3 S_{\alpha_2} + k_{\eta=-1}^{r*} \alpha_2 C_{\alpha_2} & -\zeta_3 C_{\alpha_2} + k_{\eta=-1}^{r*} \alpha_2 S_{\alpha_2} & \zeta_4 Sh_{\beta_2} + k_{\eta=-1}^{r*} \beta_2 Ch_{\beta_2} \\ -\zeta_1 C_{\alpha_2} + k_{\eta=1}^{v*} S_{\alpha_2} & \zeta_1 S_{\alpha_2} + k_{\eta=1}^{v*} C_{\alpha_2} & -\zeta_2 Ch_{\beta_2} + k_{\eta=1}^{v*} Sh_{\beta_2} \\ \zeta_3 S_{\alpha_2} + k_{\eta=1}^{r*} \alpha_2 C_{\alpha_2} & \zeta_3 C_{\alpha_2} - k_{\eta=1}^{r*} \alpha_2 S_{\alpha_2} & \zeta_4 Sh_{\beta_2} + k_{\eta=1}^{r*} \beta_2 Ch_{\beta_2} \\ -\zeta_2 Sh_{\beta_2} + k_{\eta=-1}^{v*} Ch_{\beta_2} & -\zeta_4 Ch_{\beta_2} - k_{\eta=-1}^{r*} \beta_2 Sh_{\beta_2} & \\ -\zeta_2 Sh_{\beta_2} + k_{\eta=1}^{v*} Ch_{\beta_2} & \zeta_4 Ch_{\beta_2} + k_{\eta=1}^{r*} \beta_2 Sh_{\beta_2} & \end{bmatrix} \begin{Bmatrix} B_1 \\ B_2 \\ B_3 \\ B_4 \end{Bmatrix} = \begin{Bmatrix} 0 \\ 0 \\ 0 \\ 0 \end{Bmatrix}, \quad (35)$$

205 or,

$$\mathbf{R}_y \mathbf{B} = \mathbf{0}, \quad (36)$$

<sup>206</sup> where,

$$\begin{aligned}\zeta_1 &= -\alpha_2^3 - \left( \frac{4D_{66}J_3}{\chi^2 D_{22}J_1} - \frac{D_{12}J_2}{\chi^2 D_{22}J_1} \right) \alpha_2, \\ \zeta_2 &= \beta_2^3 - \left( \frac{4D_{66}T_3}{\chi^2 D_{22}J_1} - \frac{D_{12}J_2}{\chi^2 D_{22}J_1} \right) \beta_2, \\ \zeta_3 &= -\alpha_2^2 + \frac{D_{12}J_2}{\chi^2 D_{22}J_1}, \\ \zeta_4 &= \beta_2^2 + \frac{D_{12}J_2}{\chi^2 D_{22}J_1}.\end{aligned}\tag{37}$$

<sup>207</sup> With the help of Equation (9b), the vertical displacement and rotation  
<sup>208</sup> corresponding to the mode shape  $\psi$  along the  $y$ -direction at the edges  $\eta = -1$   
<sup>209</sup> and  $\eta = 1$  can then be expressed as:

$$\begin{Bmatrix} \psi_{\eta=-1} \\ \frac{d\psi}{d\eta}_{\eta=-1} \\ \psi_{\eta=1} \\ \frac{d\psi}{d\eta}_{\eta=1} \end{Bmatrix} = \begin{bmatrix} -S_{\alpha_2} & C_{\alpha_2} & -Sh_{\beta_2} & Ch_{\beta_2} \\ \alpha_2 C_{\alpha_2}/b & \alpha_2 S_{\alpha_2}/b & \beta_2 Ch_{\beta_2}/b & -\beta_2 Sh_{\beta_2}/b \\ S_{\alpha_2} & C_{\alpha_2} & Sh_{\beta_2} & Ch_{\beta_2} \\ \alpha_2 C_{\alpha_2}/b & -\frac{\alpha_2 S_{\alpha_2}}{b} & \beta_2 Ch_{\beta_2}/b & \beta_2 Sh_{\beta_2}/b \end{bmatrix} \begin{Bmatrix} B_1 \\ B_2 \\ B_3 \\ B_4 \end{Bmatrix}, \tag{38}$$

<sup>210</sup> or,

$$\delta_y = \mathbf{Q}_y \mathbf{B}. \tag{39}$$

<sup>211</sup> Solving for the eigenvector  $\mathbf{B}$ , and then substituting into Equation (36), we  
<sup>212</sup> obtain:

$$\mathbf{R}_y \mathbf{B} = \mathbf{R}_y \mathbf{Q}_x^{-1} \delta_y = \mathbf{0}, \tag{40}$$

<sup>213</sup> where the dynamic stiffness matrix, denoted as  $\mathbf{K}_y = \mathbf{R}_y \mathbf{Q}_y^{-1}$ , can be ob-  
<sup>214</sup> tained from Equation (40).

#### <sup>215</sup> 2.4. Remarks

<sup>216</sup> (i) For the SOV methods, six independent unknown eigenvalues ( $\alpha_1, \beta_1,$   
<sup>217</sup>  $\Omega_x, \alpha_2, \beta_2, \Omega_y$ ) need to be determined for each mode shape  $\phi(\xi)\psi(\eta)$ .  
<sup>218</sup> To solve these six variables, four eigenvalue equations are provided in

219 Equations (20a), (20b), (34a) and (34b), while the remaining two trans-  
220 cendental eigenvalue equations are obtained from the determinants of  
221  $\mathbf{R}_x$  in Equation (25) for the  $x$ -direction and  $\mathbf{R}_y$  in Equation (36) for the  
222  $y$ -direction, respectively. For classical boundary conditions such as sim-  
223 ply supported (S), clamped (C), guided (G), and free (F) edges, these  
224 two transcendental equations have been simplified and summarized in  
225 previous works [53–55]. However, the process of selecting appropri-  
226 ate transcendental equations for the existing 55 different boundary-  
227 condition combinations remains tedious, and further simplification be-  
228 comes challenging when non-classical boundary conditions are applied.  
229 By simply setting the translational springs ( $k^v$ ) and rotational springs  
230 ( $k^r$ ) along the  $x$ - or  $y$ -direction edges to either zero or infinity, the  
231 classical boundary conditions can be recovered. In this case, the trans-  
232 cendental equations obtained from the determinants of  $\mathbf{R}_x$  and  $\mathbf{R}_y$  are  
233 identical to those summarized in the existing SOV methods.

234 (ii) In the existing SOV methods, numerical techniques such as the New-  
235 ton–Raphson method, homotopy method and optimization methods  
236 method have been applied to solve these six unknown variables. Al-  
237 though all six eigenvalue equations can be solved simultaneously, the  
238 computation is very expensive and convergence issues may arise [56, 57].  
239 Therefore, an iterative procedure [52, 56–59] is preferred, in which  
240 three eigenvalue equations corresponding to  $(\alpha_1, \beta_1, \Omega_x)$  and the re-  
241 maining three corresponding to  $(\alpha_2, \beta_2, \Omega_y)$  are solved separately. In  
242 fact, by substituting Equations (20a) and (20b) into the eigenvalue  
243 equation corresponding to  $\mathbf{R}_x$  and Equations (34a) and (34b) into the  
244 eigenvalue equation corresponding to  $\mathbf{R}_y$ , two highly nonlinear eigen-  
245 value equations, involving only one variable  $\Omega_x$  and  $\Omega_y$ , respectively,  
246 can be obtained. However, these equations are difficult to solve using  
247 conventional numerical methods. To address this issue, the dynamic  
248 stiffness matrices  $\mathbf{K}_x(\Omega_x)$  and  $\mathbf{K}_y(\Omega_y)$  are developed, whose determi-

249 nants are identical to the eigenvalue equations corresponding to  $\mathbf{R}_x(\Omega_x)$   
 250 and  $\mathbf{R}_y(\Omega_y)$ , respectively. In this case, the dynamic stiffness matrices  
 251  $\mathbf{K}_x(\Omega_x)$  and  $\mathbf{K}_y(\Omega_y)$  can be solved efficiently using the W–W algo-  
 252 rithm, which enhances computational robustness and ensures that no  
 253 frequencies are missed.

### 254 3. Frequency and mode shape computation

255 The dynamic stiffness matrices  $\mathbf{K}_x(\Omega_x)$  and  $\mathbf{K}_y(\Omega_y)$  serve as the eigen-  
 256 value equations for  $\Omega_x$  and  $\Omega_y$ , respectively, and a powerful W–W algorithm  
 257 based on the SOV-DSM method is introduced in Section 3.1 to compute  
 258 these eigenvalues. Section 3.2 proposes a novel technique to calculate the  
 259 mode shapes. Finally, the iterative procedure for applying the proposed  
 260 method is presented in Section 3.3.

#### 261 3.1. Wittrick–Williams algorithm and enhancement

262 The Wittrick–Williams (W–W) algorithm [91] is an effective method for  
 263 determining the natural frequencies from the dynamic stiffness matrix with  
 264 high reliability. Instead of directly solving the equations, the algorithm com-  
 265 putes the total number  $J$  of natural frequencies below a given frequency  $\omega^*$ ,  
 266 which is represented as:

$$J(\omega^*) = J_0(\omega^*) + s\{\mathbf{K}^\Delta(\omega^*)\} = J_0(\omega^*) + J_k(\omega^*), \quad (41)$$

267 where  $J_0$  represents the number of natural frequencies of the structure with  
 268 all ends fully clamped,  $\mathbf{K}^\Delta$  is the upper triangular matrix obtained from the  
 269 dynamic stiffness matrix  $\mathbf{K}$  after applying Gaussian elimination, and  $J_k(\omega^*)$   
 270 denotes the number of negative elements in the leading diagonal of  $\mathbf{K}^\Delta$ .

271 It should be noted that the  $J_0$  count is a crucial aspect when applying the  
 272 W–W algorithm. Many previous studies use a sufficiently fine mesh or enough  
 273 terms in series expansions to capture all fully clamped natural frequencies,  
 274 ensuring computational accuracy [67]. However, this approach can make the

application process cumbersome. To address this issue, the fully clamped problem can be replaced with a simply supported problem, where the Navier solution for the simply supported plate is used to count  $J_0$  [71]. Nevertheless, since analytical solutions in DSM methods involve an infinite series of Fourier terms, a sufficient number of truncation terms is required to ensure accuracy and convergence.

In fact,  $J_0$  can be indirectly determined by evaluating the number of natural frequencies  $J$  of the structure under specific boundary conditions, which are generally different from the original boundary conditions [92]:

$$J_0(p_1, \omega^*) = J(\bar{p}_1, \omega^*) - J_k(\bar{p}_1, \omega^*), \quad (42)$$

where  $p_1$  denotes the fully clamped supports, and  $\bar{p}_1$  denotes specific supports, which are typically simply supported, guided, or a combination of the two. For these specific boundary conditions, the eigenvalue equations of SOV type solution take the form of a single harmonic function. By substituting Equation (42) into Equation (41) we get the algorithm as:

$$J(p, \omega^*) = J(\bar{p}_1, \omega^*) - J_k(\bar{p}_1, \omega^*) + J_k(p, \omega^*) \quad (43)$$

where  $p$  represents the original boundary conditions of the structure. Therefore, the challenge of determining  $J_0(p_1, \omega^*)$  can be transformed into the problem of solving  $J(\bar{p}_1, \omega^*)$  instead.

By taking fully S-S boundary conditions as the basis, the eigenvalue equation corresponding to the natural frequency parameter  $\Omega_x$  can be obtained from the determinant of the coefficient matrix  $\mathbf{R}_x$  in Equation (24), as given by:

$$\sin 2\alpha_1 = 0. \quad (44)$$

With the help of Equations (20a) and (44), the closed-form solution of the  $n_x$ -th S-S boundary conditions frequency  $\Omega_{x,n_x}$  for the given  $n_y$ -order  $\psi_{n_y}(\eta)$

<sup>298</sup> can be expressed as:

$$b\Omega_{x,n_x}^4 = \left[ \left( \frac{n_x \pi}{2\chi} \right)^2 - \frac{D_{12}S_2}{D_{11}S_1} + 2 \frac{D_{66}S_3}{D_{11}S_1} \right]^2 - \left( \frac{D_{12}S_2}{D_{11}S_1} - 2 \frac{D_{66}S_3}{D_{11}S_1} \right)^2 + \frac{D_{22}S_4}{D_{11}S_1}. \quad (45)$$

<sup>299</sup> For  $\Omega_{x,n_x} \leq \Omega_x^* < \Omega_{x,n_{x+1}}$ ,  $J(\bar{p}_1, \Omega_x^*) = n_x$ .

<sup>300</sup> Similarly, the closed-form solution of the  $n_y$ -th S-S boundary conditions  
<sup>301</sup> frequency  $\Omega_{y,n_y}$  for the given  $n_x$ -order  $\phi_{n_x}(\xi)$  can be expressed as:

$$a\Omega_{y,n_y}^4 = \frac{D_{22}}{D_{11}} \left\{ \left[ \left( \frac{n_y \pi \chi}{2} \right)^2 - \frac{D_{12}T_2}{D_{22}T_1} + 2 \frac{D_{66}T_3}{D_{22}T_1} \right]^2 - \left( \frac{D_{12}T_2}{D_{22}T_1} - 2 \frac{D_{66}T_3}{D_{22}T_1} \right)^2 + \frac{D_{11}T_4}{D_{22}T_1} \right\}. \quad (46)$$

<sup>302</sup> For  $\Omega_{y,n_y} \leq \Omega_y^* < \Omega_{y,n_{y+1}}$ ,  $J(\bar{p}_1, \Omega_y^*) = n_y$ .

<sup>303</sup> It should be noted that the G-G boundary conditions have the same eigen-  
<sup>304</sup> value equations with the S-S boundary conditions, thus the G-G boundary  
<sup>305</sup> conditions frequencies can also be directly obtained from Equations (45)  
<sup>306</sup> and (46). The closed-form expression for the S-G boundary conditions can  
<sup>307</sup> be found in Appendix B.

<sup>308</sup> According to the relationships  $\Omega_x^4 = \omega_x^2 \rho h / D_{11}$  and  $\Omega_y^4 = \omega_y^2 \rho h / D_{11}$ , the  
<sup>309</sup> values of  $J(\bar{p}_1, \omega_x^*)$  and  $J(\bar{p}_1, \omega_y^*)$  can be derived from  $J(\bar{p}_1, \Omega_x^*)$  and  $J(\bar{p}_1, \Omega_y^*)$ ,  
<sup>310</sup> respectively. Therefore, this enhanced W-W algorithm can be applied to  
<sup>311</sup> estimate the lower and upper bounds of the frequency range, denoted as  $\omega_l$   
<sup>312</sup> and  $\omega_u$ , yielding an approximation for the frequency  $\omega_a \in (\omega_l, \omega_u)$  to arbitrary  
<sup>313</sup> precision.

### <sup>314</sup> 3.2. Mode shape computation

<sup>315</sup> The mode shape coefficients  $A_1$  to  $A_4$  and  $B_1$  to  $B_4$  in the eigenvectors  
<sup>316</sup> **A** and **B** for all classic boundary conditions are provided in [53, 54]. Alter-

317 natively, these coefficients can also be obtained through a simple numerical  
 318 method, which this work presents as an approach. Here, we illustrate solving  
 319 the eigenvector  $\mathbf{A}$  as an example. By assuming the exact natural frequency  
 320 as  $\omega_k$ , we can expand the coefficient matrix  $\mathbf{R}_x$  in Equation (24) using a  
 321 first-order Taylor series about  $\omega_a$ :

$$\mathbf{R}_{x,k}(\omega_k)\mathbf{A}_k = \mathbf{R}_{x,a}\mathbf{A}_k + (\omega_k - \omega_a)\mathbf{R}'_{x,a}\mathbf{A}_k + O((\omega_k - \omega_a)^2) = 0. \quad (47)$$

322 Ignoring higher-order terms, an eigenvalue problem can be derived from  
 323 Equation (47):

$$(\mathbf{R}'_{x,a})^{-1}\mathbf{R}_{x,a}\mathbf{A} = (\omega_a - \omega_k)\mathbf{A} = \tau\mathbf{A}. \quad (48)$$

324 This eigenvalue problem can be solved using the inverse iteration procedure  
 325 [94]:

$$\bar{\mathbf{A}}^{(i+1)} = \mathbf{R}_{x,a}^{-1}\mathbf{R}'_{x,a}\mathbf{A}^{(i)}, \quad (49)$$

326 where the initial guess for  $\mathbf{A}^{(0)}$  is a column vector consisting of four randomly  
 327 generated elements, each of which falls within the range (0,1). The updated  
 328 eigenvalue for the next step can be obtained as:

$$\tau^{(i+1)} = \frac{1}{\bar{A}_j^{(i+1)}}, \quad (50)$$

329 where,

$$|\bar{A}_j^{(i+1)}| = \max(|\bar{A}_1^{(i+1)}|, |\bar{A}_2^{(i+1)}|, |\bar{A}_3^{(i+1)}|, |\bar{A}_4^{(i+1)}|). \quad (51)$$

330 The updated eigenvector can be obtained as:

$$\mathbf{A}^{(i+1)} = \tau^{(i+1)}\bar{\mathbf{A}}^{(i+1)}. \quad (52)$$

The procedure can be controlled by the error tolerance  $\epsilon$  or maximum allowed steps  $i_{\max}$ :

$$\max | A_n^{(i+1)} - A_n^{(i)} | < \epsilon, \quad (53a)$$

$$i = i_{\max}. \quad (53b)$$

<sup>331</sup> Note that the mode shape coefficients  $A_1$  to  $A_4$  obtained from  $\mathbf{A}^{(i+1)}$  are  
<sup>332</sup> applied for the elastically restrained boundary conditions.

<sup>333</sup> *3.3. Numerical procedure*

<sup>334</sup> The procedure of the proposed method is as follows:

- <sup>335</sup> • **Step 1** Assume initial integral parameters  $I_1^{(0)}, I_2^{(0)}, I_3^{(0)}$ , and  $I_4^{(0)}$  in the  
<sup>336</sup>  $y$ -direction. Using the given boundary conditions at  $\xi = -1$  and  $\xi = 1$ ,  
<sup>337</sup> determine  $\mathbf{K}_x^{(0)}$  from Equation (29). Then, apply the computational  
<sup>338</sup> algorithms in Section 3.1 to compute the lower and upper bounds of the  
<sup>339</sup>  $n_x$ -th non-dimensional frequency parameter,  $2a\Omega_{l,x,n_x}^{(0)}$  and  $2a\Omega_{u,x,n_x}^{(0)}$ ,  
<sup>340</sup> and take the average  $2a\Omega_{x,n_x}^{(0)} = (2a\Omega_{l,x,n_x}^{(0)} + 2a\Omega_{u,x,n_x}^{(0)})/2$  along with its  
<sup>341</sup> corresponding mode shape  $\phi_{n_x}^{(0)}$ , where  $n_x = 1, 2, 3, \dots$ .
- <sup>342</sup> • **Step 2** Use  $\phi_{n_x}^{(0)}$  as the prescribed mode to determine  $\mathbf{K}_y^{(1)}$  in Equa-  
<sup>343</sup> tion (40), considering the boundary conditions at  $\eta = -1$  and  $\eta = 1$ .  
<sup>344</sup> Apply the computational algorithms to obtain the  $n_y$ -th frequency pa-  
<sup>345</sup> rameter  $2a\Omega_{y,n_y}^{(1)}$  and its corresponding mode shape  $\psi_{n_y}^{(1)}$ , where  $n_y =$   
<sup>346</sup>  $1, 2, 3, \dots$ . This completes the first iteration cycle.
- <sup>347</sup> • **Step 3** Use  $\psi_{n_y}^{(1)}$  as the prescribed  $n_y$ -th mode shape in the  $y$ -direction to  
<sup>348</sup> compute  $\mathbf{K}_x^{(1)}$  from Equation (29), then determine the  $n_x$ -th frequency  
<sup>349</sup> parameter  $2a\Omega_{x,n_x}^{(1)}$  and its corresponding mode shape  $\phi_{n_x}^{(1)}$ .
- <sup>350</sup> • **Step 4** Use  $\phi_{n_x}^{(1)}$  as the prescribed mode in the  $x$ -direction to com-  
<sup>351</sup> pute the  $n_y$ -th frequency parameter  $2a\Omega_{y,n_y}^{(2)}$  and its corresponding mode  
<sup>352</sup> shape  $\psi_{n_y}^{(2)}$ , completing the second iteration cycle.

- 353     • **Step 5** Stop the iteration if  $|2a\Omega_{x,n_x}^{(i)} - 2a\Omega_{x,n_x}^{(i+1)}| \leq \Delta 2a\Omega$  or  $|2a\Omega_{y,n_y}^{(i)} -$   
 354        $2a\Omega_{y,n_y}^{(i+1)}| \leq \Delta 2a\Omega$ , where  $\Delta 2a\Omega = 2a\Omega_u - 2a\Omega_l$ . Here,  $2a\Omega_l$  and  $2a\Omega_u$   
 355       are the lower and upper bounds of the frequency parameter range,  
 356       within which the actual frequency parameter  $2a\Omega$  lies, i.e.,  $2a\Omega \in$   
 357        $(2a\Omega_l, 2a\Omega_u)$ . The quantity  $\Delta 2a\Omega$  represents the frequency parame-  
 358       ter interval used in the W-W algorithm.
- 359     • **Step 6** Finally, construct the  $(n_x, n_y)$ -th mode shape as  $w(\xi, \eta) =$   
 360        $\phi_{n_x}(\xi)\psi_{n_y}(\eta)$  using Equation (8).

361     3.4. *Remarks*

- 362     (i) The traditional W-W algorithm requires a prior expression of  $J_0(p_1)$   
 363       under the C-C boundary conditions ( $p_1$ ). However, the transcendental  
 364       eigenvalue equation for C-C boundaries is complex, making it diffi-  
 365       cult to obtain a closed-form solution for the  $J_0(p_1)$  term. To overcome  
 366       this difficulty,  $J_0(p_1)$  can be indirectly determined if the  $J(\bar{p}_1)$  term is  
 367       known, where the reference boundary condition  $\bar{p}_1$  may correspond to  
 368       any other, more tractable boundary condition. Consequently, to apply  
 369       the W-W algorithm, at least one prior solution for a specific bound-  
 370       ary condition is required. Thanks to the SOV solution, the S-S, G-G,  
 371       and S-G boundary conditions yield the simplest eigenvalue equations,  
 372       involving only a single sine or cosine function. Therefore, an explicit  
 373       closed-form expression of  $J(\bar{p}_1)$  can be readily obtained when  $\bar{p}_1$  corre-  
 374       sponds to one of these boundary conditions. In numerical calculations,  
 375       to approximate infinite stiffness, the translational springs ( $k^v$ ) and ro-  
 376       tational springs ( $k^r$ ) are assigned sufficiently large values.
- 377     (ii) In the existing SOV methods, the mode shape coefficients  $A_1$  to  $A_4$  and  
 378        $B_1$  to  $B_4$  are obtained from different types of transcendental eigenvalue  
 379       equations for each boundary condition, resulting in distinct expressions  
 380       for different boundary conditions. However, the dynamic stiffness ma-  
 381       trix  $\mathbf{K}$  is applicable to all boundary conditions. Therefore, a general

382 approach is developed to compute the mode shape coefficients for arbitrary  
383 boundary conditions, and a novel yet simple numerical technique  
384 has been introduced to implement this procedure efficiently.

#### 385 4. Numerical Results

386 This section aims to validate the SOV-DSM method by comparing its  
387 results with some existing methods. In Section 4.1, the results are compared  
388 with those obtained from the extended SOV method under classical boundary  
389 conditions. In Section 4.2, the results are further compared with the finite  
390 integral transform method and numerical methods for rotationally restrained  
391 boundary conditions.

392 For all numerical calculations, the initial integral parameters are assumed  
393 as  $I_1^{(0)} = 1$ ,  $I_2^{(0)} = 1$ ,  $I_3^{(0)} = 1$ , and  $I_4^{(0)} = 10$  in the  $y$ -direction, serving as  
394 the starting point of **Step 1** for any mode in all boundary conditions.  $\bar{p}_1$  is  
395 selected as the S–S boundary condition. In this section, the interval between  
396 the upper and lower bounds of the non-dimensional frequency parameter,  
397  $2a\Delta\Omega$ , is set to 0.005, although any desired level of precision can be used.  
398 According to our numerical calculations, two iteration cycles are generally  
399 sufficient to meet the convergence requirement (i.e.,  $|2a\Omega_x^{(i)} - 2a\Omega_x^{(i+1)}| \leq$   
400  $\Delta 2a\Omega$  or  $|2a\Omega_y^{(i)} - 2a\Omega_y^{(i+1)}| \leq \Delta 2a\Omega$ ) for most cases, with at most three  
401 cycles required when applying the iterative procedure in Section 3.3.

##### 402 4.1. Classical boundary conditions

403 In this subsection, the proposed method is validated by comparison with  
404 the extended SOV method [53]. The properties of the orthotropic plate,  
405 consistent with those in [53], are as follows:  $E_1 = 185$  GPa,  $E_2 = 10.5$  GPa,  
406  $G_{12} = 7.3$  GPa,  $\rho = 1600$  kg m<sup>-3</sup>, and  $\nu_{12} = 0.28$ .

407 The translational springs ( $k^v$ ) and rotational springs ( $k^r$ ) along all edges  
408 can be set to zero or infinity (represented as  $1 \times 10^{15}$  N m<sup>-1</sup> in the numerical  
409 calculations of this study) to obtain different classic boundary conditions.

410 The results for SSSS, SCSF, GCGC, CCCC, SSCC, SCCC, GGCC, CCFF,  
 411 CFCF, CFFF, and FFFF boundary conditions are presented in Tables 1  
 412 to 3. These results demonstrate high accuracy compared to the extended  
 413 SOV method, with difference remaining smaller than the frequency parame-  
 414 ter interval  $2a\Delta\Omega = 0.005$ . The frequency parameters in both directions are  
 415 equal ( $2a\Omega_x - 2a\Omega_y = 0$ ) in almost all cases, with a few exceptions where  
 416  $2a\Omega_x - 2a\Omega_y = 0.005$ . In fact, higher accuracy compared to the extended  
 417 SOV method can be achieved if the frequency parameter interval  $2a\Delta\Omega$  is  
 418 set smaller than 0.005. It should be noted that the accuracy improves only  
 419 by reducing  $2a\Delta\Omega$ , and no additional iterations are required according to  
 420 our calculations. Section 4.1 shows the first six nonzero mode shapes of a  
 421 square orthotropic plate with FFFF boundary conditions, where the mode  
 422 shape coefficients are calculated using the numerical method developed in  
 423 this study. Instead of selecting fixed expressions for the mode shape coeffi-  
 424 cients based on specific boundary conditions, our method is applicable to all  
 425 boundary conditions.

426 *4.2. Rotational spring-supported edges*

In this subsection, rectangular orthotropic plates with rotational spring-  
 supported edges with no translations ( $k_\xi^v = k_\eta^v = \infty$ ) are examined. The  
 dimensionless rotational stiffness coefficients are defined as:

$$r_\xi = \frac{2ak_\xi^r}{D_{11}}, \quad (54a)$$

$$r_\eta = \frac{2bk_\eta^r}{D_{22}}. \quad (54b)$$

427 The first example considers a square isotropic plate with all four edges ro-  
 428 tationally restrained. The vertical translational springs along the four edges  
 429 are numerically set as  $k_{\xi=-1}^v = k_{\xi=1}^v = k_{\eta=-1}^v = k_{\eta=1}^v = 1 \times 10^{12}$  N m<sup>-1</sup>. The  
 430 material properties are given as  $D_{11} = D_{22} = D_3$  and  $v_{12} = v_{21} = 0.3$ .

431 Section 4.2 presents the frequency parameter  $2a\Omega$  for different rotational

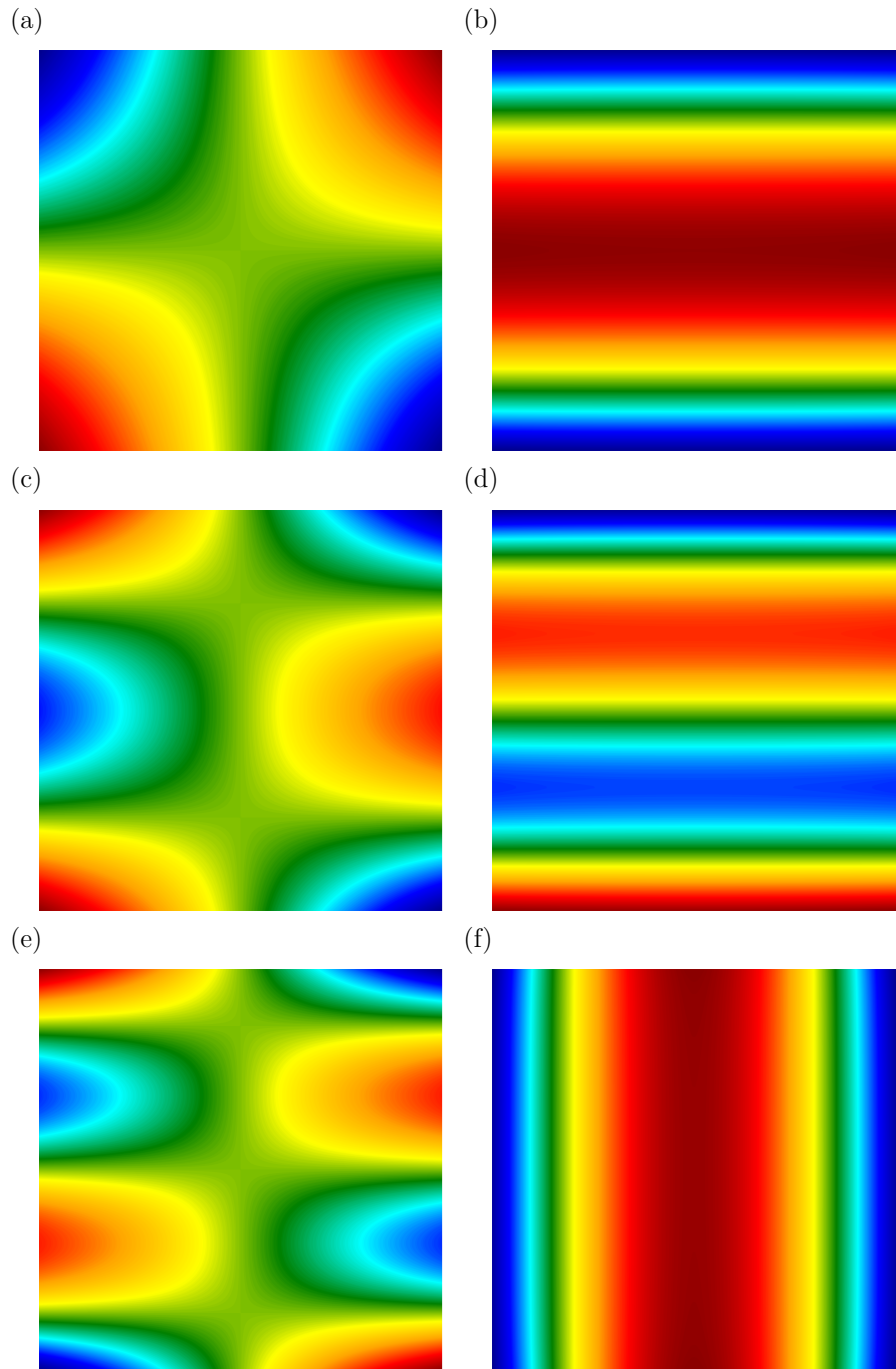


Figure 2: The first six nonzero mode shapes of a square orthotropic plate with FFFF boundary conditions: (a) the first mode; (b) the second mode; (c) the third mode; (d) the fourth mode; (e) the fifth mode; (f) the sixth mode.

Table 1: The first seven frequency parameter  $2a\Omega$  of orthotropic rectangular plates with SSSS, SCSF and GCGC boundary conditions.

BCs	$\chi$	Mode	$2a\Omega_x = 2a\Omega_y = 2a\sqrt[4]{\rho h \omega^2 / D_{11}}$						
			1	2	3	4	5	6	7
SSSS	0.5	Mode number	(1,1)	(1,2)	(1,3)	(1,4)	(1,5)	(1,6)	(1,7)
		extended SOV 53	3.1807	3.3190	3.5938	4.0135	4.5495	5.1635	5.8265
		Present	3.1825	3.3225	3.5975	4.0175	4.5525	5.1625	5.8275
	1	Mode number	(1,1)	(1,2)	(1,3)	(2,1)	(1,4)	(2,2)	(2,3)
		extended SOV 53	3.3190	4.0135	5.1635	6.3615	6.5200	6.6379	7.1876
		Present	3.3175	4.0175	5.1625	6.3625	6.5175	6.6375	7.1875
	1.5	Mode number	(1,1)	(1,2)	(2,1)	(2,2)	(1,3)	(2,3)	(1,4)
		extended SOV 53	3.5938	5.1635	6.4698	7.1876	7.2331	8.5389	9.4352
		Present	3.5975	5.1675	6.4725	7.1875	7.2325	8.5375	9.4375
SCSF	0.5	Mode number	(1,1)	(1,2)	(1,3)	(1,4)	(1,5)	(1,6)	(1,7)
		extended SOV 53	3.1516	3.2451	3.4588	3.8131	4.2950	4.8711	5.5087
		Present	3.1525	3.2475	3.4575	3.8175	4.2925	4.8725	5.5075
	1	Mode number	(1,1)	(1,2)	(1,3)	(1,4)	(2,1)	(2,2)	(2,3)
		extended SOV 53	3.1908	3.6428	4.5972	5.8599	6.3033	6.4901	6.9177
		Present	3.1925	3.6425	4.5975	5.8575	6.3025	6.4925	6.9175
	1.5	Mode number	(1,1)	(1,2)	(1,3)	(2,1)	(2,2)	(2,3)	(1,4)
		extended SOV 53	3.2710	4.3430	6.2157	6.3337	6.8043	7.8718	8.3518
		Present	3.2725	4.3425	6.2175	6.3325	6.8025	7.8725	8.3525
GCGC	0.5	Mode number	(1,1)	(1,2)	(1,3)	(2,1)	(2,2)	(1,4)	(2,3)
		extended SOV 53	1.1544	1.9166	2.6835	3.1983	3.3890	3.4501	3.7372
		Present	1.1525	1.9175	2.6825	3.1975	3.3875	3.4525	3.7375
	1	Mode number	(1,1)	(2,1)	(1,2)	(2,2)	(1,3)	(2,3)	(3,1)
		extended SOV 53	2.3087	3.4900	3.8331	4.4682	5.3669	5.7736	6.3967
		Present	2.3075	3.4875	3.8325	4.4675	5.3675	5.7725	6.3975
	1.5	Mode number	(1,1)	(2,1)	(1,2)	(2,2)	(3,1)	(3,2)	(1,3)
		extended SOV 53	3.4631	4.1353	5.7497	6.0981	6.6049	7.6449	8.0504
		Present	3.4625	4.1325	5.7475	6.0975	6.6075	7.6425	8.0525

Table 2: The first seven frequency parameter  $2a\Omega$  of orthotropic rectangular plates with CCCC, SSCC, SCCC and GGCC boundary conditions.

BCs	$\chi$	Mode	$2a\Omega_x = 2a\Omega_y = 2a\sqrt[4]{\rho h \omega^2 / D_{11}}$						
			1	2	3	4	5	6	7
CCCC	0.5	Mode number	(1,1)	(1,2)	(1,3)	(1,4)	(1,5)	(1,6)	(1,7)
		extended SOV 53	4.7500	4.8208	4.9682	5.2177	5.5791	6.0430	6.5892
		Present	4.7475	4.8225	4.9725	5.2175	5.5825	6.0425	6.5875
	1	Mode number	(1,1)	(1,2)	(1,3)	(1,4)	(2,1)	(2,2)	(2,3)
		extended SOV 53	4.8579	5.3546	6.2819	7.4972	7.9193	8.1490	8.6054
		Present	4.8575	5.3575	6.2875	7.4975	7.9175	8.1475	8.6075
	1.5	Mode number	(1,1)	(1,2)	(2,1)	(1,3)	(2,2)	(2,3)	(1,4)
		extended SOV 53	5.1581	6.5412	8.0409	8.4945	8.7204	9.9793	10.6460
		Present	5.1575	6.5375	8.0425	8.4975	8.7175	9.9775	10.6425
SSCC	0.5	Mode number	(1,1)	(1,2)	(1,3)	(1,4)	(1,5)	(1,6)	(1,7)
		extended SOV 53	3.9542	4.0520	4.2525	4.5785	5.0254	5.5682	6.1789
		Present	3.9575	4.0525	4.2475	4.5775	5.0225	5.5725	6.1825
	1	Mode number	(1,1)	(1,2)	(1,3)	(1,4)	(2,1)	(2,2)	(2,3)
		extended SOV 53	4.0745	4.6606	5.7009	6.9940	7.1396	7.3894	7.8881
		Present	4.0775	4.6625	5.7025	6.9925	7.1375	7.3875	7.8875
	1.5	Mode number	(1,1)	(1,2)	(2,1)	(1,3)	(2,2)	(2,3)	(1,4)
		extended SOV 53	4.3602	5.8384	7.2531	7.8560	7.9481	9.2515	10.0366
		Present	4.3625	5.8325	7.2525	7.8575	7.9525	9.2525	10.0325
SCCC	0.5	Mode number	(1,1)	(1,2)	(1,3)	(1,4)	(1,5)	(1,6)	(1,7)
		extended SOV 53	3.9596	4.0745	4.3027	4.6606	5.1361	5.7009	6.3271
		Present	3.9575	4.0725	4.3025	4.6625	5.1325	5.7025	6.3325
	1	Mode number	(1,1)	(1,2)	(1,3)	(2,1)	(1,4)	(2,2)	(2,3)
		extended SOV 53	4.1349	4.8478	5.9805	7.1541	7.3192	7.4478	8.0121
		Present	4.1325	4.8475	5.9825	7.1525	7.3175	7.4475	8.0125
	1.5	Mode number	(1,1)	(1,2)	(2,1)	(2,2)	(1,3)	(2,3)	(3,1)
		extended SOV 53	4.5824	6.2766	7.3116	8.1528	8.3705	9.5986	10.3507
		Present	4.5825	6.2775	7.3125	8.1525	8.3725	9.5975	10.3525
GGCC	0.5	Mode number	(1,1)	(1,2)	(1,3)	(1,4)	(1,5)	(1,6)	(1,7)
		extended SOV 53	2.3750	2.4841	2.7895	3.2946	3.9226	4.6123	5.3326
		Present	2.3725	2.4875	2.7925	3.2975	3.9225	4.6075	5.3325
	1	Mode number	(1,1)	(1,2)	(1,3)	(2,1)	(2,2)	(1,4)	(2,3)
		extended SOV 53	2.4290	3.1410	4.4293	5.5202	5.7315	5.8801	6.2606
		Present	2.4325	3.1425	4.4325	5.5225	5.7325	5.8775	6.2625
	1.5	Mode number	(1,1)	(1,2)	(2,1)	(2,2)	(1,3)	(2,3)	(3,1)
		extended SOV 53	2.5790	4.2472	5.5565	6.1533	6.4347	7.5231	8.6732
		Present	2.5825	4.2475	5.5575	6.1525	6.4325	7.5225	8.6725

Table 3: The first seven nonzero frequency parameter  $2a\Omega$  of orthotropic rectangular plates with CCFF, CFCF, CFFF and FFFF boundary conditions.

BCs	$\chi$	Mode	$2a\Omega_x = 2a\Omega_y = 2a\sqrt[4]{\rho h \omega^2 / D_{11}}$						
			1	2	3	4	5	6	7
CCFF	0.5	Mode number	(1,1)	(1,2)	(1,3)	(1,4)	(1,5)	(1,6)	(2,1)
		extended SOV 53	1.8978	2.0905	2.4925	3.0563	3.7110	4.4117	4.7029
		Present	1.8975	2.0925	2.4925	3.0575	3.7125	4.4125	4.7025
	1	Mode number	(1,1)	(1,2)	(1,3)	(2,1)	(2,2)	(1,4)	(2,3)
		extended SOV 53	1.9930	2.7895	4.0733	4.7338	5.0652	5.5128	5.7419
		Present	1.9925	2.7875	4.0725	4.7325	5.0675	5.5125	5.7425
	1.5	Mode number	(1,1)	(1,2)	(2,1)	(2,2)	(1,3)	(2,3)	(3,1)
		extended SOV 53	2.1780	3.7411	4.7931	5.5758	5.8895	7.0263	7.9006
		Present	2.1775	3.7425	4.7925	5.5725	5.8875	7.0275	7.9025
CFCF	0.5	Mode number	(1,1)	(1,2)	(1,3)	(1,4)	(1,5)	(1,6)	(1,7)
		extended SOV 53	4.7297	4.7427	4.7881	4.8819	5.0478	5.3072	5.6694
		Present	4.7275	4.7425	4.7875	4.8825	5.0475	5.3075	5.6675
	1	Mode number	(1,1)	(1,2)	(1,3)	(1,4)	(1,5)	(1,6)	(2,1)
		extended SOV 53	4.7295	4.7817	5.0012	5.5348	6.4407	7.6182	7.8523
		Present	4.7275	4.7825	5.0025	5.5325	6.4425	7.6175	7.8525
	1.5	Mode number	(1,1)	(1,2)	(1,3)	(1,4)	(2,1)	(2,2)	(2,3)
		extended SOV 53	4.7292	4.8458	5.4221	6.7635	7.8518	7.9470	8.3021
		Present	4.7275	4.8475	5.4225	6.7625	7.8525	7.9475	8.3025
CFFF	0.5	Mode number	(1,1)	(1,2)	(1,3)	(1,4)	(1,5)	(1,6)	(1,7)
		extended SOV 53	1.8751	1.9439	2.1679	2.5657	3.1106	3.7486	4.4382
		Present	1.8775	1.9425	2.1675	2.5675	3.1125	3.7475	4.4375
	1	Mode number	(1,1)	(1,2)	(1,3)	(1,4)	(2,1)	(2,2)	(2,3)
		extended SOV 53	1.8750	2.1242	2.9077	4.1319	4.6937	4.8226	5.2263
		Present	1.8775	2.1225	2.9075	4.1325	4.6925	4.8225	5.2275
	1.5	Mode number	(1,1)	(1,2)	(1,3)	(2,1)	(2,2)	(2,3)	(1,4)
		extended SOV 53	1.8750	2.3402	3.8522	4.6935	4.9753	5.8314	5.9292
		Present	1.8775	2.3425	3.8525	4.6925	4.9775	5.8325	5.9275
FFFF	0.5	Mode number	(1,3)	(2,2)	(1,4)	(2,3)	(1,5)	(2,4)	(2,5)
		extended SOV 53	1.1540	1.4858	1.9157	2.1704	2.6821	2.7881	3.4093
		Present	1.1525	1.4875	1.9175	2.1725	2.6825	2.7875	3.4075
	1	Mode number	(2,2)	(1,3)	(2,3)	(1,4)	(2,4)	(3,1)	(3,2)
		extended SOV 53	2.1311	2.3082	3.2734	3.8320	4.4962	4.7298	4.9138
		Present	2.1325	2.3075	3.2725	3.8325	4.4975	4.7275	4.9125
	1.5	Mode number	(2,2)	(1,3)	(2,3)	(3,1)	(3,2)	(1,4)	(3,3)
		extended SOV 53	2.6277 <sup>30</sup>	3.4625	4.2915	4.7296	5.1259	5.7485	6.1588
		Present	2.6275	3.4625	4.2925	4.7275	5.1275	5.7475	6.1575

432 stiffness coefficients  $r_\xi = r_\eta$  with values 0.1, 1, 10, 100, and 1000. Notably,  
433 when  $r_\xi = r_\eta = 0$  and  $r_\xi = r_\eta = \infty$ , the boundary conditions correspond to  
434 SSSS and CCCC, respectively.

435 Interestingly, the results indicate that the frequencies  $\Omega_x$  and  $\Omega_y$  are not  
436 strictly equal for some mode shapes under these boundary conditions. The  
437 actual frequency  $\Omega$  lies between  $\Omega_x$  and  $\Omega_y$ , which may be attributed to the  
438 fact that  $\Omega_x$  and  $\Omega_y$  satisfy Rayleigh's principle in Equation (3), represent-  
439 ing the weak-form governing equations, but do not necessarily satisfy the  
440 strong-form governing equations in Equation (1). For a physical problem  
441 with exact solutions, both Equations (1) and (3) must be satisfied. If this  
442 condition is not met, applying Equation (3) still provides a viable approach  
443 for approximating the exact solution of the plate. Thus, the exact frequency  
444 can be estimated as  $\Omega = (\Omega_x + \Omega_y)/2$ . As shown in Section 4.2, the maxi-  
445 mum difference between  $\Omega$  and the analytical solutions of the finite integral  
446 transform method reported in 95 is less than 1.3%. Figure 3 illustrates the  
447 variation in mode shapes corresponding to the fundamental natural frequency  
448 as the rotational stiffness  $r_\xi = r_\eta$  increases from zero to  $\infty$ , transitioning the  
449 boundary conditions from SSSS to CCCC.

450 The next example considers a rectangular orthotropic plate with three  
451 simply supported edges ( $k_{\xi=-1}^r = k_{\xi=1}^r = k_{\eta=1}^r = 0$ ), while the edge at  $\eta = -1$   
452 is rotationally restrained. The material properties are consistent with those  
453 in 95, where  $2D_{11} = 2D_{22} = D_3$  and  $\nu_{12} = \nu_{21} = 0.3$ . Table 4 shows the  
454 fundamental frequency results for different length ratios ( $b/a$ ), comparing  
455 them with those reported in 95. The maximum observed difference is 0.8%  
456 when  $r_{\eta=-1} = 10$ .

457 Interestingly, in certain numerical calculations involving rotationally re-  
458 strained boundary conditions, the variables  $\alpha_1$  and  $\alpha_2$  may take complex  
459 values rather than being purely real. Consequently, the mode shape coeffi-  
460 cients  $A_1$ ,  $A_2$ ,  $B_1$ , and  $B_2$  become complex-valued, leading to  $\mathbf{R}$  and  $\mathbf{Q}^{-1}$   
461 being complex matrices. However, the mode shapes  $\phi(\xi)$  and  $\psi(\eta)$  remain

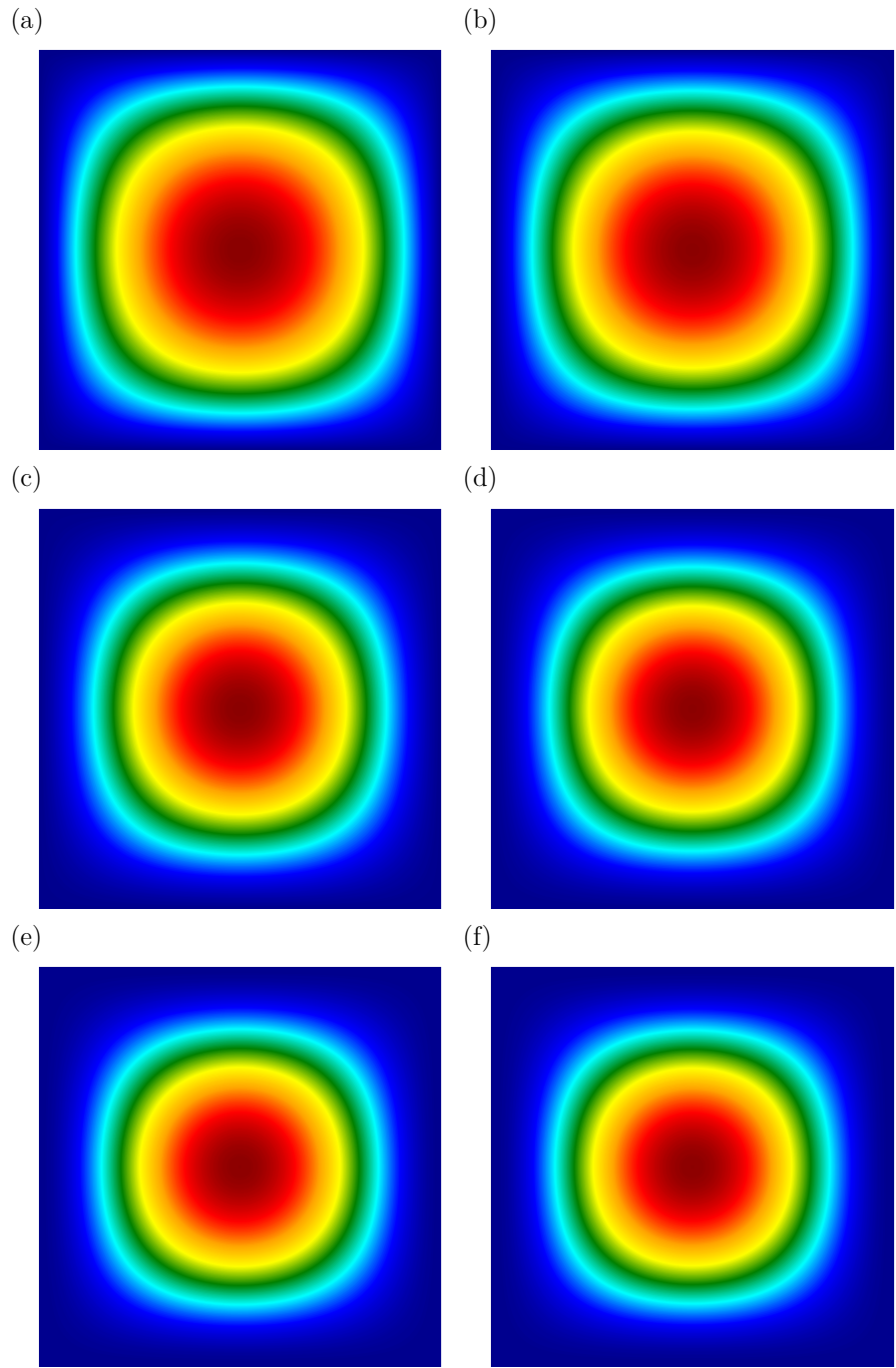


Figure 3: The first vibration mode shapes of a square isotropic plate with all four edges rotationally restrained, shown for different dimensionless rotational stiffness values  $r_\xi = r_\eta$ . (a)  $r_\xi = r_\eta = 0$  (simply supported); (b)  $r_\xi = r_\eta = 1$  (light rotational restraint); (c)  $r_\xi = r_\eta = 10$  (moderate restraint); (d)  $r_\xi = r_\eta = 20$ ; (e)  $r_\xi = r_\eta = 100$  (firmly clamped); (f)  $r_\xi = r_\eta = \infty$  (perfectly clamped edges).

$r$	Mode	$2a\Omega$					
		1	2	3	4	5	6
0.1	Mode number	(1,1)	(1,2)	(2,1)	(2,2)	(1,3)	(3,1)
	Ref.96	4.454	6.992	7.045	8.890	9.782	9.960
	Ref.95	4.465	7.039	7.039	8.897	9.945	9.945
	Present ( $\Omega_x$ )	4.463	7.028	7.043	8.893	9.938	9.953
	Present ( $\Omega_y$ )	4.463	7.043	7.028	8.893	9.953	9.938
	Present ( $\Omega$ )	4.463	7.035	7.035	8.893	9.945	9.945
	Difference (%)	0.044	0.056	0.056	0.044	0.000	0.000
1	Mode number	(1,1)	(1,2)	(2,1)	(2,2)	(3,1)	(1,3)
	Ref.96	4.529	7.008	7.136	8.936	9.787	10.036
	Ref.95	4.637	7.155	7.155	8.991	10.029	10.030
	Present ( $\Omega_x$ )	4.648	7.098	7.223	8.993	10.093	9.968
	Present ( $\Omega_y$ )	4.648	7.223	7.098	8.993	9.968	10.098
	Present ( $\Omega$ )	4.648	7.160	7.160	8.993	10.030	10.033
	Difference (%)	0.237	0.069	0.069	0.022	0.009	0.029
10	Mode number	(1,1)	(1,2)	(2,1)	(2,2)	(1,3)	(3,1)
	Ref.95	5.346	7.768	7.768	9.537	10.552	10.563
	Present ( $\Omega_x$ )	5.413	7.718	7.953	9.598	10.448	10.782
	Present ( $\Omega_y$ )	5.413	7.953	7.718	9.598	10.782	10.453
	Present ( $\Omega$ )	5.413	7.835	7.835	9.598	10.615	10.618
	Difference (%)	1.253	0.862	0.862	0.639	0.597	0.520
	Mode number	(1,1)	(1,2)	(2,1)	(2,2)	(1,3)	(3,1)
100	Ref.96	5.895	8.326	8.422	10.167	10.957	11.297
	Ref.95	5.901	8.442	8.442	10.253	11.307	11.333
	Present ( $\Omega_x$ )	5.913	8.428	8.473	10.258	11.293	11.373
	Present ( $\Omega_y$ )	5.913	8.473	8.478	10.258	11.373	11.293
	Present ( $\Omega$ )	5.913	8.450	8.450	10.258	11.333	11.333
	Difference (%)	0.203	0.094	0.094	0.048	0.229	0.000
	Mode number	(1,1)	(1,2)	(2,1)	(2,2)	(1,3)	(3,1)
1000	Ref.95	6.011	8.585	8.585	10.424	11.495	11.522
	Present ( $\Omega_x$ )	5.988	8.553	8.553	10.388	11.463	11.478
	Present ( $\Omega_y$ )	5.988	8.553	8.553	10.388	11.478	11.463
	Present ( $\Omega$ )	5.988	8.553	8.553	10.388	11.470	11.470
	Difference (%)	0.382	0.372	0.372	0.345	0.217	0.451

<sup>462</sup> real-valued, and the dynamic stiffness matrix  $\mathbf{K} = \mathbf{RQ}^{-1}$  is a real symmetric  
<sup>463</sup> matrix. Thus, the frequency  $\Omega$  can be obtained by solving  $\mathbf{K}$  using this  
<sup>464</sup> enhanced W-W algorithm provided in this study, which avoids solving the  
<sup>465</sup> eigenvalue equations in both the real and complex domains.

Table 4: Fundamental frequency parameter  $2a\Omega = 2a\sqrt[4]{\rho h\omega^2/D_{11}}$  of rectangular orthotropic plates with three edges simply supported ( $k_{\xi=-1}^r = k_{\xi=1}^r = k_{\eta=1}^r = 0$ ) and the edge at  $\eta = -1$  rotationally restrained.

		2aΩ				
$b/a$	$r_{\eta=-1}$	Ref.95	Present ( $\Omega$ )	Present ( $\Omega_x$ )	Present ( $\Omega_y$ )	Difference (%)
0.5	0	7.530	7.523	7.523	7.523	0.092
	1	7.690	7.700	7.588	7.813	0.130
	10	8.250	8.308	8.198	8.418	0.703
	$\infty$	8.705	8.695	8.695	8.695	0.114
1.0	0	4.917	4.918	4.918	4.918	0.020
	1	4.954	4.960	4.933	4.988	0.121
	10	5.114	5.128	5.088	5.168	0.273
	$\infty$	5.289	5.278	5.278	5.278	0.207
1.5	0	4.126	4.128	4.128	4.128	0.048
	1	4.139	4.138	4.128	4.148	0.024
	10	4.202	4.208	4.188	4.228	0.142
	$\infty$	4.292	4.288	4.288	4.288	0.093

## <sup>466</sup> 5. Conclusion

<sup>467</sup> In this study, a separation-of-variables dynamic stiffness matrix method  
<sup>468</sup> (SOV-DSM) has been developed for the vibration analysis of orthotropic rect-  
<sup>469</sup> angular plates with general homogeneous boundary conditions. The bound-  
<sup>470</sup> ary conditions of the SOV-type plate are extended to homogeneous elasti-  
<sup>471</sup> cally restrained boundaries beyond the classical cases, resulting in two more  
<sup>472</sup> complex eigenvalue equations. Existing SOV methods face the challenge of

473 solving six unknown variables ( $\alpha_1$ ,  $\beta_1$ ,  $\Omega_x$ ,  $\alpha_2$ ,  $\beta_2$ ,  $\Omega_y$ ) through six eigen-  
474 value equations, which leads to high computational cost and convergence  
475 difficulties. To address this, dynamic stiffness matrices are formulated based  
476 on the SOV-type plate, and an enhanced Wittrick–Williams (W–W) algo-  
477 rithm is introduced to solve these matrices regardless of the complexity of  
478 the highly nonlinear eigenvalue equations derived from them. This enhanced  
479 W–W algorithm resolves the well-known  $J_0$  problem by providing an explicit  
480 closed-form expression for the  $J_0$  term, derived from the characteristics of  
481 SOV-type plates. Furthermore, a novel yet simple numerical technique is  
482 proposed for mode shape calculation, making it applicable to all boundary  
483 conditions.

484 Classical boundary conditions, such as guided, simply supported, clamped,  
485 and free edges, can be realized by setting the translational springs ( $k^v$ ) and  
486 rotational springs ( $k^r$ ) along the plate edges to either zero or infinity, as ap-  
487 propriate. Numerical experiments validate the high accuracy of this approach  
488 for these boundary conditions. The results shows that the SOV solution can  
489 also be extended to handle elastically restrained boundary conditions. De-  
490 spite certain approximations inherent in few elastically restrained cases, the  
491 maximum percentage error across all numerical experiments remains within  
492 1.25%. This may occur because the SOV solution used is derived from the  
493 weak-form governing equation, which is based on Rayleigh’s principle.

494 As a closed-form dynamic stiffness formulation, this approach has the  
495 potential to construct more concise and lower-dimensional dynamic stiffness  
496 matrices for orthotropic rectangular plate assemblies compared to existing  
497 DSM approaches.

<sup>498</sup> **Appendix A Integral parameters**

<sup>499</sup> The integral parameters  $I_1$ ,  $I_2$ ,  $I_3$ , and  $I_4$  are defined as follows:

$$\begin{aligned} I_1 &= \int_0^1 \psi^2 d\eta \\ &= (B_1^2 + B_2^2 - B_3^2 + B_4^2) + \frac{-B_1^2 + B_2^2}{2\alpha_2} \sin(2\alpha_2) + \frac{B_3^2 + B_4^2}{2\beta_2} \sinh(2\beta_2) \\ &\quad + \frac{4(\alpha_2 B_2 B_4 + \beta_2 B_1 B_3)}{\alpha_2^2 + \beta_2^2} \sin(\alpha_2) \cosh(\beta_2) \\ &\quad + \frac{4(-\alpha_2 B_1 B_3 + \beta_2 B_2 B_4)}{\alpha_2^2 + \beta_2^2} \cos(\alpha_2) \sinh(\beta_2). \end{aligned} \tag{A.1}$$

<sup>500</sup>

$$\begin{aligned} I_2 &= \int_0^1 \left( \psi \frac{d^2\psi}{d\eta^2} \right) d\eta \\ &= (-\alpha_2^2 B_1^2 - \alpha_2^2 B_2^2 - \beta_2^2 B_3^2 + \beta_2^2 B_4^2) \\ &\quad + \frac{\alpha_2(B_1^2 - B_2^2)}{2} \sin(2\alpha_2) + \frac{\beta_2(B_3^2 + B_4^2)}{2} \sinh(2\beta_2) \\ &\quad + \frac{2(-\alpha_2^2 + \beta_2^2)(\alpha_2 B_2 B_4 + \beta_2 B_1 B_3)}{\alpha_2^2 + \beta_2^2} \sin(\alpha_2) \cosh(\beta_2) \\ &\quad + \frac{2(-\alpha_2^2 + \beta_2^2)(-\alpha_2 B_1 B_3 + \beta_2 B_2 B_4)}{\alpha_2^2 + \beta_2^2} \cos(\alpha_2) \sinh(\beta_2). \end{aligned} \tag{A.2}$$

<sup>501</sup>

$$\begin{aligned} I_3 &= \int_0^1 \left( \frac{d\psi}{d\eta} \right)^2 d\eta \\ &= \alpha_2^2 B_1^2 + \alpha_2^2 B_2^2 + \beta_2^2 B_3^2 - \beta_2^2 B_4^2 \\ &\quad + \frac{\alpha_2(B_1^2 - B_2^2)}{2} \sin(2\alpha_2) + \frac{\beta_2(B_3^2 + B_4^2)}{2} \sinh(2\beta_2) \\ &\quad + \frac{4\alpha_2\beta_2(\alpha_2 B_1 B_3 - \beta_2 B_2 B_4)}{\alpha_2^2 + \beta_2^2} \sin(\alpha_2) \cosh(\beta_2) \\ &\quad + \frac{4\alpha_2\beta_2(\alpha_2 B_2 B_4 + \beta_2 B_1 B_3)}{\alpha_2^2 + \beta_2^2} \cos(\alpha_2) \sinh(\beta_2). \end{aligned} \tag{A.3}$$

502

$$\begin{aligned}
I_4 &= \int_0^1 \left( \frac{d^2\psi}{d\eta^2} \right)^2 d\eta \\
&= \left( \alpha_2^4 B_1^2 + \alpha_2^4 B_2^2 - \beta_2^4 B_3^2 + \beta_2^4 B_4^2 \right) \\
&\quad + \frac{\alpha_2^3(-B_1^2 + B_2^2)}{2} \sin(2\alpha_2) + \frac{\beta_2^3(B_3^2 + B_4^2)}{2} \sinh(2\beta_2) \\
&\quad + \frac{4\alpha_2^2\beta_2^2(-\alpha_2 B_2 B_4 - \beta_2 B_1 B_3)}{\alpha_2^2 + \beta_2^2} \sin(\alpha_2) \cosh(\beta_2) \\
&\quad + \frac{4\alpha_2^2\beta_2^2(\alpha_2 B_1 B_3 - \beta_2 B_2 B_4)}{\alpha_2^2 + \beta_2^2} \cos(\alpha_2) \sinh(\beta_2)
\end{aligned} \tag{A.4}$$

503 The integral parameters  $J_1$ ,  $J_2$ ,  $J_3$ , and  $J_4$  can be obtained by replacing  $B_1$   
504 to  $B_4$  by  $A_1$  to  $A_4$ , respectively, and  $\alpha_2$  and  $\beta_2$  by  $\alpha_1$  and  $\beta_1$ , respectively.

505 **Appendix B  $J(\bar{p}_1)$  count for S-G boundary conditions**

If the S-G boundary conditions are selected as the specific boundary conditions to solve the  $J(\bar{p}_1, \omega^*)$ , then, from the eigenvalue equations in the  $x$ - and  $y$ -directions,

$$\cos 2\alpha_1 = 0, \tag{B.1a}$$

$$\cos 2\alpha_2 = 0, \tag{B.1b}$$

506 the closed-form solution of the  $n_x$ -th S-G boundary conditions  $\Omega_{x,n_x}$  for the  
507 given  $n_y$ -order  $\psi_{n_y}(\eta)$ , can be expressed as

$$\begin{aligned}
b\Omega_{x,n_x}^4 &= \left[ \frac{1}{\chi^2} \left( \frac{n_x\pi}{2} - \frac{\pi}{4} \right)^2 - \frac{D_{12}S_2}{D_{11}S_1} + 2\frac{D_{66}S_3}{D_{11}S_1} \right]^2 \\
&\quad - \left( \frac{D_{12}S_2}{D_{11}S_1} - 2\frac{D_{66}S_3}{D_{11}S_1} \right)^2 + \frac{D_{22}S_4}{D_{11}S_1},
\end{aligned} \tag{B.2}$$

508 and the closed-form solution of the  $n_y$ -th S-G boundary conditions frequency  
 509  $\Omega_{y,n_y}$  for the given  $n_x$ -order  $\phi_{n_x}(\xi)$  can be obtained as:

$$a\Omega_{y,n_y}^4 = \frac{D_{22}}{D_{11}} \left\{ \left[ \chi^2 \left( \frac{n_y \pi}{2} - \frac{\pi}{4} \right)^2 - \frac{D_{12}T_2}{D_{22}T_1} + 2 \frac{D_{66}T_3}{D_{22}T_1} \right]^2 - \left( \frac{D_{12}T_2}{D_{22}T_1} - 2 \frac{D_{66}T_3}{D_{22}T_1} \right)^2 + \frac{D_{11}T_4}{D_{22}T_1} \right\}. \quad (\text{B.3})$$

510

## 511 References

- 512 [1] M. E. Biancolini, C. Brutti, L. Reccia, Approximate solution for free  
 513 vibrations of thin orthotropic rectangular plates, Journal of Sound and  
 514 Vibration 288 (1-2) (2005) 321–344. doi:10.1016/j.jsv.2005.01.005.
- 515 [2] L. Navier, Extrait des recherches sur la flexion des plans élastiques, Bull.  
 516 Sci. Soc. Philomat. (1823) 95–102.
- 517 [3] M. Levy, Sur l'équilibre élastique d'une plaque rectangulaire, Comptes  
 518 Rendus Acad. Sci. Paris 129 (1899) 535–539.
- 519 [4] A. W. Leissa, The free vibration of rectangular plates, Journal of Sound  
 520 and Vibration 31 (3) (1973) 257–293. doi:10.1016/S0022-460X(73)  
 521 80371-2.
- 522 [5] K. Y. Lam, K. C. Hung, S. T. Chow, Vibration analysis of plates with  
 523 cutouts by the modified rayleigh-ritz method, Applied Acoustics 28 (1)  
 524 (1989) 49–60. doi:10.1016/0003-682X(89)90030-3.
- 525 [6] S. Zhao, J. Sun, X. Ma, J. Sun, Y. An, K. Li, T. Wang, Free vibration  
 526 analysis of thin rectangular plates with mixed point support conditions  
 527 using the rayleigh–ritz method, Journal of Aerospace Engineering 38 (5)  
 528 (2025) 04025067. doi:10.1061/JAEEZ.ASENG-6193.

- 529 [7] R. Jain, M. S. Azam, P. P. Singh, Bending analysis of functionally graded  
530 plates resting on elastic foundation: A rayleigh-ritz approach and ann  
531 method, *Mechanics of Advanced Materials and Structures* 31 (29) (2024)  
532 11484–11502. doi:[10.1080/15376494.2024.2307474](https://doi.org/10.1080/15376494.2024.2307474).
- 533 [8] A. Bagheri, A. Mortezaei, M. A. Sayarinejad, Analysis of free in-plane vi-  
534 brations of a rectangular plate with various boundary conditions canon-  
535 ical form using the modified riley-ritz method, *Results in Engineering*  
536 21 (2024) 101768. doi:[10.1016/j.rineng.2024.101768](https://doi.org/10.1016/j.rineng.2024.101768).
- 537 [9] P. A. Laura, B. F. Saffell Jr, Study of small-amplitude vibrations  
538 of clamped rectangular plates using polynomial approximations, *The  
539 Journal of the Acoustical Society of America* 41 (4A) (1967) 836–839.  
540 doi:[10.1121/1.1910414](https://doi.org/10.1121/1.1910414).
- 541 [10] P. Krysl, T. Belytschko, Analysis of thin plates by the element-free  
542 galerkin method, *Computational Mechanics* 17 (1) (1995) 26–35. doi:  
543 [10.1007/BF00356476](https://doi.org/10.1007/BF00356476).
- 544 [11] H. Ma, J. Chen, J. Deng, Analysis of the dynamic response for kirch-  
545 hoff plates by the element-free galerkin method, *Journal of Compu-  
546 tational and Applied Mathematics* 451 (2024) 116093. doi:[10.1016/j.cam.2024.116093](https://doi.org/10.1016/j.cam.2024.116093).
- 548 [12] H. Ma, J. Chen, J. Deng, Error analysis of the element-free galerkin  
549 method for a nonlinear plate problem, *Computers & Mathematics with  
550 Applications* 163 (2024) 56–65. doi:[10.1016/j.camwa.2024.03.020](https://doi.org/10.1016/j.camwa.2024.03.020).
- 551 [13] M. S. Pereira, M. V. Donadon, Modified consistent element-free galerkin  
552 method applied to reissner–mindlin plates, *Thin-Walled Structures* 212  
553 (2025) 113185. doi:[10.1016/j.tws.2025.113185](https://doi.org/10.1016/j.tws.2025.113185).
- 554 [14] Y. Zhao, K. Yuan, B. Qin, L. Shen, Z. Wang, A fast polynomial-fe  
555 method for the vibration of the composite laminate quadrilateral plates

- 556 and shells based on the segmentation strategy, Composite Structures  
557 338 (2024) 118035. doi:10.1016/j.compstruct.2024.118035.
- 558 [15] Y. Yang, M. J. Kingan, B. R. Mace, Analysis of the forced response  
559 of coupled panels using a hybrid finite element/wave and finite element  
560 method, Journal of Sound and Vibration 537 (2022) 117174. doi:10.  
561 1016/j.jsv.2022.117174.
- 562 [16] R. R. Paccola, M. S. M. Sampaio, H. B. Coda, Continuous stress dis-  
563 tribution following transverse direction for fem orthotropic laminated  
564 plates and shells, Applied Mathematical Modelling 40 (15-16) (2016)  
565 7382–7409. doi:10.1016/j.apm.2016.03.005.
- 566 [17] E. Carrera, D. Scano, Finite elements based on jacobi shape functions  
567 for the free vibration analysis of beams, plates, and shells, Mechanics of  
568 Advanced Materials and Structures 31 (1) (2024) 4–12. doi:10.1080/  
569 15376494.2023.2219438.
- 570 [18] C. Yang, J. Nakaoka, S. Hirose, Semi-analytical fem for modelling 3d  
571 guided waves scattering in an infinite plate, Applied Mathematical Mod-  
572elling (2025) 116236doi:10.1016/j.apm.2025.116236.
- 573 [19] Z. Ding, Natural frequencies of rectangular plates using a set of static  
574 beam functions in rayleigh-ritz method, Journal of Sound and Vibration  
575 189 (1) (1996) 81–87. doi:10.1006/jsvi.1996.0006.
- 576 [20] K. Y. Cheung, D. Zhou, The free vibrations of tapered rectangular plates  
577 using a new set of beam functions with the rayleigh–ritz method, Journal  
578 of Sound and Vibration 223 (5) (1999) 703–722. doi:10.1006/jsvi.  
579 1998.2160.
- 580 [21] Y. K. Cheung, D. Zhou, The free vibrations of rectangular compos-  
581 itive plates with point-supports using static beam functions, Compos-

- 582 ite Structures 44 (2-3) (1999) 145–154. doi:10.1016/S0263-8223(98)  
583 00122-6.
- 584 [22] D. Zhou, Vibrations of point-supported rectangular plates with variable  
585 thickness using a set of static tapered beam functions, International  
586 Journal of Mechanical Sciences 44 (1) (2002) 149–164. doi:10.1016/  
587 S0020-7403(01)00081-9.
- 588 [23] R. B. Bhat, Natural frequencies of rectangular plates using characteris-  
589 tic orthogonal polynomials in rayleigh-ritz method, Journal of Sound  
590 and Vibration 102 (4) (1985) 493–499. doi:10.1016/S0022-460X(85)  
591 80109-7.
- 592 [24] X. Xie, G. Jin, An efficient domain decomposition approach for the free  
593 and forced vibration analysis of plate assemblies, Thin-Walled Struc-  
594 tures (2025) 113621doi:10.1016/j.tws.2025.113621.
- 595 [25] Z. Celep, Z. Özcan, A. Güner, Elastic triangular plate dynamics on uni-  
596 lateral winker foundation: Analysis using chebyshev polynomial ex-  
597 pansion for forced vibrations, Journal of Mechanical Science and Technology  
598 39 (1) (2025) 65–79. doi:10.1007/s12206-024-1207-5.
- 599 [26] N. Madinier, Q. Leclère, K. Ege, A. Berry, Spatial and frequency identi-  
600 fication of the dynamic properties of thin plates with the frequency-  
601 adapted virtual fields method, Journal of Sound and Vibration 596  
602 (2025) 118760. doi:10.1016/j.jsv.2024.118760.
- 603 [27] X. Sun, R. Gao, Y. Zhang, Spectral stochastic isogeometric analysis of  
604 bending and free vibration of porous functionally graded plates, Ap-  
605 plied Mathematical Modelling 116 (2023) 711–734. doi:10.1016/j.  
606 apm.2022.12.017.
- 607 [28] C. P. Filipich, M. B. Rosales, Arbitrary precision frequencies of a free

- 608        rectangular thin plate, *Journal of Sound and Vibration* 230 (3) (2000)  
609        521–539. [doi:10.1006/jsvi.1999.2629](https://doi.org/10.1006/jsvi.1999.2629).
- 610 [29] Y. V. S. Kumar, J. K. Paik, Buckling analysis of cracked plates using hi-  
611        erarchical trigonometric functions, *Thin-Walled Structures* 42 (5) (2004)  
612        687–700. [doi:10.1016/j.tws.2003.12.012](https://doi.org/10.1016/j.tws.2003.12.012).
- 613 [30] G. A. Yessenbayeva, F. M. Akhanov, T. K. Makazhanova, On the cal-  
614        culation of rectangular plates by the trigonometric series, *Bulletin of*  
615        *the Karaganda University. Mathematics Series* 94 (2) (2019) 115–120.  
616        [doi:10.31489/2019M2/115-120](https://doi.org/10.31489/2019M2/115-120).
- 617 [31] G. He, D. Cao, J. Wei, Y. Cao, Z. Chen, Study on analytical global  
618        modes for a multi-panel structure connected with flexible hinges, *Ap-  
619        plied Mathematical Modelling* 91 (2021) 1081–1099. [doi:10.1016/j.apm.2020.10.044](https://doi.org/10.1016/j.apm.2020.10.044).
- 621 [32] J. Su, W. He, K. Zhang, Q. Zhang, Y. Qu, Vibration analysis of func-  
622        tionally graded porous cylindrical shells filled with dense fluid using an  
623        energy method, *Applied Mathematical Modelling* 108 (2022) 167–188.  
624        [doi:10.1016/j.apm.2022.03.028](https://doi.org/10.1016/j.apm.2022.03.028).
- 625 [33] W. L. Li, Vibration analysis of rectangular plates with general elastic  
626        boundary supports, *Journal of Sound and Vibration* 273 (3) (2004) 619–  
627        635. [doi:10.1016/S0022-460X\(03\)00562-5](https://doi.org/10.1016/S0022-460X(03)00562-5).
- 628 [34] Y. K. Cheung, D. Zhou, Vibrations of moderately thick rectangular  
629        plates in terms of a set of static timoshenko beam functions, *Computers  
630        & Structures* 78 (6) (2000) 757–768. [doi:10.1016/S0045-7949\(00\)00058-4](https://doi.org/10.1016/S0045-7949(00)<br/>631        00058-4).
- 632 [35] D. Zhou, Vibrations of mindlin rectangular plates with elastically re-  
633        strained edges using static timoshenko beam functions with the rayleigh–

- ritz method, International Journal of Solids and Structures 38 (32-33) (2001) 5565–5580. doi:10.1016/S0020-7683(00)00384-X.
- [36] L. E. Monterrubio, S. Ilanko, Proof of convergence for a set of admissible functions for the rayleigh–ritz analysis of beams and plates and shells of rectangular planform, Computers & Structures 147 (2015) 236–243. doi:10.1016/j.compstruc.2014.09.008.
- [37] F. C. Onyeka, B. O. Mama, C. D. Nwa-David, Application of variation method in three dimensional stability analysis of rectangular plate using various exact shape functions, Nigerian Journal of Technology 41 (1) (2022) 8–20. doi:10.4314/njt.v41i1.2.
- [38] L. V. Kantorovich, V. I. Krylov, Approximate Methods of Higher Analysis, Interscience Publishers, New York, 1958.
- [39] A. D. Kerr, An extension of the kantorovich method, Quarterly of Applied Mathematics 26 (2) (1968) 219–229. doi:10.1090/qam/99857.
- [40] A. D. Kerr, H. Alexander, An application of the extended kantorovich method to the stress analysis of a clamped rectangular plate, Acta Mechanica 6 (2) (1968) 180–196. doi:10.1007/BF01170382.
- [41] H. Rostami, A. R. Ranji, F. Bakhtiari-Nejad, Free in-plane vibration analysis of rotating rectangular orthotropic cantilever plates, International Journal of Mechanical Sciences 115 (2016) 438–456. doi:10.1016/j.ijmecsci.2016.07.030.
- [42] B. Huang, H. S. Kim, Interlaminar stress analysis of piezo-bonded composite laminates using the extended kantorovich method, International Journal of Mechanical Sciences 90 (2015) 16–24. doi:10.1016/j.ijmecsci.2014.11.003.
- [43] I. Shufrin, M. Eisenberger, Semi-analytical modeling of cutouts in rectangular plates with variable thickness–free vibration analysis, Applied

- 661 Mathematical Modelling 40 (15-16) (2016) 6983–7000. doi:10.1016/j.apm.2016.02.020.
- 662
- 663 [44] A. Singh, P. Kumari, Three-dimensional free vibration analysis of composite fgm rectangular plates with in-plane heterogeneity: An ekm solution, International Journal of Mechanical Sciences 180 (2020) 105711. doi:10.1016/j.ijmecsci.2020.105711.
- 664
- 665
- 666
- 667 [45] W.-X. Zhong, A new systematic methodology for theory of elasticity, Dalian University of Technology Press, Dalian (1995) 182–187.
- 668
- 669 [46] Y. Xing, B. Liu, New exact solutions for free vibrations of rectangular thin plates by symplectic dual method, Acta Mechanica Sinica 25 (2009) 265–270. doi:10.1007/s10409-008-0208-4.
- 670
- 671
- 672 [47] C. W. Lim, C. F. Lü, Y. Xiang, W. Yao, On new symplectic elasticity approach for exact free vibration solutions of rectangular kirchhoff plates, International Journal of Engineering Science 47 (1) (2009) 131–140. doi:10.1016/j.ijengsci.2008.08.003.
- 673
- 674
- 675
- 676 [48] Y. Shi, D. An, Z. Wu, L. Liang, L. Chen, R. Li, Symplectic analytical solutions for free vibration of elastically line-hinged orthotropic rectangular plates with rotationally restrained edges, Applied Mathematical Modelling 136 (2024) 115629. doi:10.1016/j.apm.2024.08.001.
- 677
- 678
- 679
- 680 [49] D. Xu, J. Xu, S. Xiong, L. Chen, Q. He, B. Wang, R. Li, Hamiltonian system-based analytic thermal buckling solutions of orthotropic rectangular plates, International Journal of Mechanical Sciences 267 (2024) 108987. doi:10.1016/j.ijmecsci.2024.108987.
- 681
- 682
- 683
- 684 [50] Y. Shi, D. An, Z. Hu, Z. Zhou, R. Li, Free vibration solutions of rotationally restrained stepped thick rectangular plates utilizing a symplectic analytical framework, Applied Mathematical Modelling 143 (2025) 116044. doi:10.1016/j.apm.2025.116044.
- 685
- 686
- 687

- 688 [51] Y. F. Xing, B. Liu, New exact solutions for free vibrations of thin or-  
689 thotropic rectangular plates, *Composite Structures* 89 (4) (2009) 567–  
690 574. doi:[10.1016/j.compstruct.2008.11.010](https://doi.org/10.1016/j.compstruct.2008.11.010).
- 691 [52] Y. Xing, Q. Sun, B. Liu, Z. Wang, The overall assessment of closed-  
692 form solution methods for free vibrations of rectangular thin plates,  
693 *International Journal of Mechanical Sciences* 140 (2018) 455–470. doi:  
694 [10.1016/j.ijmecsci.2018.03.013](https://doi.org/10.1016/j.ijmecsci.2018.03.013).
- 695 [53] Y. Xing, Z. Wang, An extended separation-of-variable method for  
696 the free vibration of orthotropic rectangular thin plates, *International*  
697 *Journal of Mechanical Sciences* 182 (2020) 105739. doi:[10.1016/j.ijmecsci.2020.105739](https://doi.org/10.1016/j.ijmecsci.2020.105739).
- 699 [54] Y. Xing, Z. Wang, An improved separation-of-variable method for the  
700 free vibration of orthotropic rectangular thin plates, *Composite Struc-*  
701 *tures* 252 (2020) 112664. doi:[10.1016/j.compstruct.2020.112664](https://doi.org/10.1016/j.compstruct.2020.112664).
- 702 [55] Y. Xing, G. Li, Y. Yuan, A review of the analytical solution methods  
703 for the eigenvalue problems of rectangular plates, *International Journal*  
704 *of Mechanical Sciences* 221 (2022) 107171. doi:[10.1016/j.ijmecsci.2022.107171](https://doi.org/10.1016/j.ijmecsci.2022.107171).
- 706 [56] Z. Wang, Y. Xing, G. Li, Closed-form solutions for the free vibrations of  
707 three-dimensional orthotropic rectangular plates, *International Journal*  
708 *of Mechanical Sciences* 199 (2021) 106398. doi:[10.1016/j.ijmecsci.2021.106398](https://doi.org/10.1016/j.ijmecsci.2021.106398).
- 710 [57] Z. Wang, Y. Xing, An extended separation-of-variable method for free  
711 vibrations of orthotropic rectangular thin plate assemblies, *Thin-Walled*  
712 *Structures* 169 (2021) 108491. doi:[10.1016/j.tws.2021.108491](https://doi.org/10.1016/j.tws.2021.108491).
- 713 [58] Z. Wang, Y. Xing, Q. Sun, Y. Yang, Highly accurate closed-  
714 form solutions for free vibration and eigenbuckling of rectangular

- 715       nanoplates, Composite Structures 210 (2019) 822–830. doi:10.1016/  
716       j.compstruct.2018.11.094.
- 717 [59] Z. Wang, Y. Xing, Q. Sun, Highly accurate closed-form solutions for the  
718       free in-plane vibration of rectangular plates with arbitrary homogeneous  
719       boundary conditions, Journal of Sound and Vibration 470 (2020) 115166.  
720       doi:10.1016/j.jsv.2019.115166.
- 721 [60] J. R. Banerjee, Dynamic stiffness formulation for structural elements:  
722       a general approach, Computers & Structures 63 (1997) 101–103. doi:  
723       10.1016/S0045-7949(96)00326-4.
- 724 [61] S. O. Papkov, J. R. Banerjee, Dynamic stiffness formulation and free  
725       vibration analysis of specially orthotropic mindlin plates with arbitrary  
726       boundary conditions, Journal of Sound and Vibration 458 (2019) 522–  
727       543. doi:10.1016/j.jsv.2019.06.028.
- 728 [62] X. Liu, S. Tao, X. Zhao, X. Liu, Z. Lu, F. Liu, Dynamic response analysis  
729       for bridges subjected to moving vehicle loads by using the analytical  
730       dynamic stiffness method, Computers & Structures 292 (2024) 107240.  
731       doi:10.1016/j.compstruc.2023.107240.
- 732 [63] M. Boscolo, J. Banerjee, Dynamic stiffness elements and their applica-  
733       tions for plates using first order shear deformation theory, Computers &  
734       Structures 89 (3-4) (2011) 395–410. doi:10.1016/j.compstruc.2010.  
735       11.005.
- 736 [64] F. Fazzolari, M. Boscolo, J. Banerjee, An exact dynamic stiffness ele-  
737       ment using a higher order shear deformation theory for free vibration  
738       analysis of composite plate assemblies, Composite Structures 96 (2013)  
739       262–278. doi:10.1016/j.compstruct.2012.08.033.
- 740 [65] O. Ghorbel, J.-B. Casimir, L. Hammami, I. Tawfiq, M. Haddar, Dy-

- 741 namic stiffness formulation for free orthotropic plates, Journal of Sound  
742 and Vibration 346 (2015) 361–375. doi:10.1016/j.jsv.2015.02.020.
- 743 [66] F. W. Williams, H. J. Ouyang, D. Kennedy, C. B. York, Wave propa-  
744 gation along longitudinally periodically supported or stiffened prismatic  
745 plate assemblies, Journal of Sound and Vibration 186 (2) (1995) 197–  
746 205. doi:10.1006/jsvi.1995.0443.
- 747 [67] J. Banerjee, S. Papkov, X. Liu, D. Kennedy, Dynamic stiffness matrix of  
748 a rectangular plate for the general case, Journal of Sound and Vibration  
749 342 (2015) 177–199. doi:10.1016/j.jsv.2014.12.031.
- 750 [68] X. Liu, J. Banerjee, Free vibration analysis for plates with arbi-  
751 trary boundary conditions using a novel spectral-dynamic stiffness  
752 method, Computers & Structures 164 (2016) 108–126. doi:10.1016/j.  
753 compstruc.2015.11.005.
- 754 [69] X. Liu, W. Zhou, M. Filippi, Y. Wang, A wavenumber dynamic stiff-  
755 ness method for exact and efficient dispersion analysis of plate built-  
756 up waveguides, Journal of Sound and Vibration 591 (2024) 118605.  
757 doi:10.1016/j.jsv.2024.118605.
- 758 [70] W. Zhou, X. Liu, Y. Wang, X. Zhao, Wavenumber dynamic stiffness  
759 formulation for exact dispersion analysis of moderately thick symmetric  
760 cross-ply laminated plate built-up waveguides, Thin-Walled Structures  
761 204 (2024) 112305. doi:10.1016/j.tws.2024.112305.
- 762 [71] X. Liu, J. Banerjee, An exact spectral-dynamic stiffness method for free  
763 flexural vibration analysis of orthotropic composite plate assemblies—  
764 part i: Theory, Composite Structures 132 (2015) 1274–1287. doi:10.  
765 1016/j.comstruct.2015.07.020.
- 766 [72] S. Timoshenko, Theory of Plates and Shells, McGraw-Hill Book Com-  
767 pany, 1940.

- 768 [73] D. J. Gorman, Free in-plane vibration analysis of rectangular plates  
769 with elastic support normal to the boundaries, *Journal of Sound and*  
770 *Vibration* 285 (4-5) (2005) 941–966. doi:10.1016/j.jsv.2004.09.017.
- 771 [74] Y. Mochida, S. Ilanko, Transient vibration analysis of a completely free  
772 plate using modes obtained by gorman’s superposition method, *Journal*  
773 *of Sound and Vibration* 329 (10) (2010) 1890–1900. doi:10.1016/j.  
774 jsv.2009.11.029.
- 775 [75] B. Wang, P. Li, R. Li, Symplectic superposition method for new analytic  
776 buckling solutions of rectangular thin plates, *International Journal of*  
777 *Mechanical Sciences* 119 (2016) 432–441. doi:10.1016/j.ijmecsci.  
778 2016.11.006.
- 779 [76] Z. Hu, X. Zheng, D. An, C. Zhou, Y. Yang, R. Li, New analytic buck-  
780 ling solutions of side-cracked rectangular thin plates by the symplectic  
781 superposition method, *International Journal of Mechanical Sciences* 191  
782 (2021) 106051. doi:10.1016/j.ijmecsci.2020.106051.
- 783 [77] Z. Wang, D. Xu, J. Li, Z. Hu, G. Gong, R. Li, New analytical buck-  
784 ling solutions for non-lévy-type graphene-reinforced composite lami-  
785 nated plates, *Composite Structures* 360 (2025) 119067. doi:10.1016/  
786 j.compstruct.2025.119067.
- 787 [78] H. Khov, W. L. Li, R. F. Gibson, An accurate solution method for  
788 the static and dynamic deflections of orthotropic plates with general  
789 boundary conditions, *Composite Structures* 90 (4) (2009) 474–481. doi:  
790 10.1016/j.compstruct.2009.04.020.
- 791 [79] W. L. Li, X. Zhang, J. Du, Z. Liu, An exact series solution for the  
792 transverse vibration of rectangular plates with general elastic boundary  
793 supports, *Journal of Sound and Vibration* 321 (1-2) (2009) 254–269.  
794 doi:10.1016/j.jsv.2008.09.035.

- 795 [80] Y. M. Grigorenko, L. S. Rozhok, Discrete fourier-series method in  
796 problems of bending of variable-thickness rectangular plates, Journal  
797 of Engineering Mathematics 46 (3) (2003) 269–280. doi:10.1023/A:  
798 1025076708442.
- 799 [81] Q. Wang, D. Shi, Q. Liang, F. Ahad, An improved fourier series solution  
800 for the dynamic analysis of laminated composite annular, circular, and  
801 sector plate with general boundary conditions, Journal of Composite  
802 Materials 50 (30) (2016) 4199–4233. doi:10.1177/00219983166352.
- 803 [82] B. Leng, S. Ullah, T. Yu, K. Li, New analytical free vibration solutions  
804 of thin plates using the fourier series method, Applied Sciences 12 (17)  
805 (2022) 8631. doi:10.3390/app12178631.
- 806 [83] R. Li, Y. Zhong, B. Tian, Y. Liu, On the finite integral transform method  
807 for exact bending solutions of fully clamped orthotropic rectangular thin  
808 plates, Applied Mathematics Letters 22 (12) (2009) 1821–1827. doi:  
809 10.1016/j.aml.2009.07.003.
- 810 [84] Y. Zhong, X.-F. Zhao, R. Li, Free vibration analysis of rectangular can-  
811 tilever plates by finite integral transform method, International Journal  
812 for Computational Methods in Engineering Science and Mechanics 14 (3)  
813 (2013) 221–226. doi:10.1080/15502287.2012.711424.
- 814 [85] B. Tian, R. Li, Y. Zhong, Integral transform solutions to the bend-  
815 ing problems of moderately thick rectangular plates with all edges free  
816 resting on elastic foundations, Applied Mathematical Modelling 39 (1)  
817 (2015) 128–136. doi:10.1016/j.apm.2014.05.012.
- 818 [86] S. Zhang, L. Xu, Bending of rectangular orthotropic thin plates with ro-  
819 tationally restrained edges: a finite integral transform solution, Applied  
820 Mathematical Modelling 46 (2017) 48–62. doi:10.1016/j.apm.2017.  
821 01.053.

- 822 [87] Y. Chen, D. An, C. Zhou, Y. Li, J. Xu, R. Li, Analytical free vibration  
823 solutions of rectangular edge-cracked plates by the finite integral trans-  
824 form method, International Journal of Mechanical Sciences 243 (2023)  
825 108032. doi:10.1016/j.ijmecsci.2022.108032.
- 826 [88] B. Li, H. Liu, J. Liu, M. Cui, X. Gao, J. Lv, A novel weak-form mesh-  
827 less method based on lagrange interpolation for mechanical analysis of  
828 complex thin plates, Engineering Analysis with Boundary Elements 169  
829 (2024) 106021. doi:10.1016/j.enganabound.2024.106021.
- 830 [89] Z. Zhu, Y. Song, Y. Zhang, Q. Liu, G. Wang, Sound radiation of the  
831 plate with arbitrary holes, International Journal of Mechanical Sciences  
832 264 (2024) 108814. doi:10.1016/j.ijmecsci.2023.108814.
- 833 [90] D. Shao, B. Li, Analytic vibration solutions for moving-loaded compos-  
834 ite plates beyond lévy boundaries, International Journal of Mechanical  
835 Sciences (2025) 110547doi:10.1016/j.ijmecsci.2025.110547.
- 836 [91] W. H. Wittrick, F. W. Williams, A general algorithm for comput-  
837 ing natural frequencies of elastic structures, The Quarterly Journal  
838 of Mechanics and Applied Mathematics 24 (3) (1971) 263–284. doi:  
839 10.1093/qjmmam/24.3.263.
- 840 [92] F. Han, D. Dan, W. Cheng, J. Zang, An improved wittrick-williams  
841 algorithm for beam-type structures, Composite Structures 204 (2018)  
842 560–566. doi:10.1016/j.compstruct.2018.07.108.
- 843 [93] X. Liu, L. Chang, J. R. Banerjee, H.-C. Dan, Closed-form dynamic  
844 stiffness formulation for exact modal analysis of tapered and functionally  
845 graded beams and their assemblies, International Journal of Mechanical  
846 Sciences 214 (2022) 106887. doi:10.1016/j.ijmecsci.2021.106887.
- 847 [94] S. Yuan, K. Ye, F. Williams, Second order mode-finding method in dy-

- 848 namic stiffness matrix methods, Journal of Sound and Vibration 269 (3-  
849 5) (2004) 689–708. doi:10.1016/S0022-460X(03)00126-3.
- 850 [95] S. Zhang, L. Xu, R. Li, New exact series solutions for transverse vibra-  
851 tion of rotationally-restrained orthotropic plates, Applied Mathematical  
852 Modelling 65 (2019) 348–360. doi:10.1016/j.apm.2018.08.033.
- 853 [96] M. Mukhopadhyay, Free vibration of rectangular plates with edges hav-  
854 ing different degrees of rotational restraint, Journal of Sound and Vi-  
855 bration 67 (4) (1979) 459–468. doi:10.1016/0022-460X(79)90438-3.